originates from the nearshore occurrences and not from remote offshore areas.

Acknowledgments

References

Fernando, L. J. D., 1948, The geology and mineral deposits of Ceylon: *Imp.Inst.* (London) *Bull.*, Vol. 46, pp. 303–325.

Fernando, L. J. D., 1970, The geology and mineral resources of Ceylon: UNESCO/ECAFE Second Seminar on Geochemical Exploration Methods and Techniques Suited to the Humid, Tropic Environment, Peradeniya, Ceylon, 10–20 September, 1970, document GSM (2)/110, 29 pp.

Geological Survey Department of Ceylon, 1968, Mineral Map of Ceylon: Ceylon Geol. Survey Dept., map, 1:1, 520, 640.

Hess, G., 1980, Placer Prospection off Pulmoddai, Sri Lanka; preliminary ore reserve calculation, Preussag AG, Metallgesellschaft AG, March 1980, 20 pp., unpublished.

Hess, G., and Westenberger, H., 1980, Placer Prospection off Pulmoddai, Sri Lanka; chemical and mineralogical investigation and ilmenite, rutile and zircon content, Preussag AG, Metallgesellschaft AG, May 1980, 32 pp., 19 fig., unpublished.

Meyer, K., 1979, Placer Prospection off Pulmoddai, Sri Lanka, preliminary report, Preussag AG, Metallgesellschaft AG, May 1979, 25 pp., unpublished.

Meyer, K., 1979, Placer Prospection off Pulmoddai, Sri Lanka, Vibrocoring, Preussag AG, Metallgesellschaft AG, November 1979, 19 pp., unpublished.

Overstreet, W. C., 1972, Ilmenite beach placer, Pulmoddai, Ceylon, and ilmenite resources of the pleistocene and holocene formations of Ceylon, U.S. Geological Survey, open file report No. 1757, 70 pp.

Shekarchi, E., 1967, The mineral industry of Ceylon, in *U.S. Bur. Mines Minerals Yearbook*, 1965, Vol. 4, pp. 1063–1066.

Morphological and Geochemical Characteristics of Manganese Nodules Collected from Three Areas on an Equatorial Pacific Transect by R. V. *Sonne*

G. Friedrich., G. P. Glasby,* T. Thijssen, and W. L. Plüger

Abteilung für Angewandte Lagerstättenlehre der RWTH, D-5100 Aachen
Federal Republic of Germany

Abstract   Manganese nodules collected from three areas (*C*, *F*, and *G*) on a N–S equatorial Pacific transect at 134° W by R. V. *Sonne* show differences in size, morphology, surface density and composition which can best be interpreted in terms of the biogenic theory of nodule formation.

Area *C* (11°30′ N) is a zone of siliceous ooze between the Clarion and Clipperton Fracture Zones and is characterized by the presence of two discrete nodule populations: larger "mature" nodules and smaller "immature" nodules. The nodules are characterized by high Mn:Fe ratios (average 5.4) and high Ni + Cu contents (average 2.48%), large size (average nodule weight 92.6 g) and high abundance (average 4.9 kg/m²). Area *F* (7° S) is a zone of siliceous debris-rich calcareous ooze. The nodules are mostly

*Permanent Address: New Zealand Oceanographic Institute, D.S.I.R., Wellington, New Zealand.

small and are characterized by high Mn:Fe ratios (average 4.8) and high Ni + Cu contents (average 2.54%) small size (average nodule weight 2.4 g) and low abundance (average 1.3 kg/m²). Area *G* (10° S) is a zone of siliceous debris-rich calcareous ooze. The area is tectonically active and the main graben of the Marquesas Fracture Zone runs through the area at 10° S. The nodules display a complex morphology and· are characterized by lower Mn:Fe ratios (average 2.2) and lower Ni + Cu contents (average 1.81%), small size (average nodule weight 2.5 g) and intermediate abundance (average 3.1 kg/m²). All three areas are characterized by wide variations in nodule densities over limited distances. In areas *C* and *F*, nodule morphology is dependent principally on nodule size, there being a progressive flattening of the nodules and development of equatorial rims with increasing nodule size. At area *G*, nodule morphology is rendered more complex by three additional factors; the in situ fragmentation of the nodules on the seafloor resulting from lines of weakness (septuarian cracks) on the nodule surface; the presence of angular volcanic rock fragments, particularly immediately south of the main graben of the Marquesas Fracture Zone; and the tendency towards polynucleate nodule formation which is enhanced by the presence of abundant nodule and volcanic rock fragments. Nodules containing these volcanic rock fragments (mainly from south of the graben) are characterized by lower Mn, Cu, and Ni and higher Fe contents than those in which they are absent (mainly from north of the graben). The tectonics of the area therefore influence both the "seeding" and the composition of these nodules.

From a comparison of the nodules collected from both the northern and southern margins of the belt of equatorial high productivity, it is concluded that the erosive bottom water conditions existing between the Clarion and Clipperton Fracture Zones since the lower Miocene have resulted in a combination of highly biogenic (siliceous) sediments with low sedimentation rates. This in turn has permitted the development of mature nodules with high Mn:Fe ratios and high Ni + Cu contents (resulting from the biogenic influence) and high surface densities (resulting from the low sedimentation rates). It is the combination of these two characteristics which gives the nodules from the equatorial North Pacific their economic potential. The higher sedimentation rates at the southern margins of the belt of equatorial high productivity (due to the less erosive bottom water conditions) have resulted in

the formation of smaller nodules with lower surface densities. Despite their high Mn:Fe ratios and Ni + Cu contents, these nodules appear to be of lesser economic potential.

There are two principal sources of elements in nodules from the equatorial zone: pore water and seawater. The pore water contribution is a diagenetic phenomenon whose characteristics are controlled by the decomposition of siliceous organisms in the sediment column rather than by the redox characteristics of the metals involved. This pore-water contribution leads to a faster growth rate, enrichment of Mn, Ni, Cu, Zn, Ba, Mo, and Tl in the nodule, and differences in sphericity and surface texture of the underside of the nodule compared with the upper surface. The enrichment sequence for metals in the nodules derived from pore water relative to those derived from seawater is Cu > Ni > Zn > Mo $\approx$ Mn > Tl $\approx$ Ba. The enrichment of the divalent metals in the nodules from the equatorial Pacific leads to the stabilization (and therefore formation) of todorokite rather than δ - MnO_2 as the principal manganese oxide phase in these nodules, although it usually occurs in conjunction with δ - MnO_2.

The relative contributions of pore water and seawater to nodule growth are also a function of nodule diameter. Smaller nodules tend to be spheroidal with uniform surface texture on all sides; with increasing size, the nodules become progressively flatter and have different surface texture on both sides. This reflects the fact that the rolling characteristics of the nodules are related to approximately the third power of nodule diameter. Smaller nodules therefore tend to be deposited in a uniform milieu because their rate of rolling on the seafloor is faster than their growth rate; larger nodules which are more static on the seafloor have characteristics that indicate deposition of elements from seawater on the upper surface and from pore water on the lower surface. The situation in these regions of high biological productivity is quite different from those prevailing in regions of low biological productivity such as beneath the subtropical anticyclonic gyres (i.e., red clay regions) where this contribution from a metal-enriched pore water is much reduced.

These data indicate that the biogenic hypothesis is central to an understanding of manganese nodule genesis in the equatorial Pacific and in particular influences the nodule shape, surface texture, rate of growth, composition, and mineralogy. The nodule characteristics in this region are also influenced by the hydrologi-

cal characteristics of the bottom water, sedimentation rates, local geological and tectonic conditions (including seeding effects), and topography.

Introduction

In a recent publication, Craig (1979) has shown the extreme usefulness of a careful examination of the distribution of a large number of manganese nodules collected from a series of locations in the equatorial North Pacific between the Clarion and Clipperton Fracture Zones in assessing the genesis of these nodules. Such a statistical treatment of data is invaluable in comparing nodule populations from different areas quantitatively and it is clear that such an approach is needed to replace the more traditional approach in which individual authors consider isolated nodules from different locations by a range of chemical and mineralogical techniques without classifying the nodules in a systematic way. The advantage of a universally accepted nodule classification scheme is that all data, no matter where collected and by whom, can be compared directly. There is an overwhelming need for such an approach in future regional surveys where precise comparisons of nodule populations between areas are required. The use of the older, arbitrary classification schemes for nodules such as those of Meyer (1973), Uchio (1976), Moritani et al. (1977), Halbach and Özkara (1979), Piper et al. (1979a), Usui (1979), Mallik (1980), Mizuno (1981) and Moritani and Nakao (1981) should be discontinued.

During the International Cooperative Investigations of Manganese Nodule Environments (I.C.I.M.E.) Project, a total of 9,529 nodules were collected by R. V. *Sonne* in mid-1978 from three areas (*C*, *F* and *G*) on a N–S equatorial Pacific transect at 134° W. The nodules have been described by a modification of the Meylan and Craig classification which was previously used by Bäcker et al. (1976), Meylan et al. (1978), and Craig (1979). A series of nodules from each size class at each station has been chemically analyzed. The purpose of this paper is to describe the principal morphological, mineralogical, and geochemical characteristics of the nodules from each of these areas quantitatively and to present comments on

their mode of formation based on these data. The data for each area are described in turn. Preliminary results of this cruise have been presented by Friedrich et al. (1979, 1981). A detailed comparison of the relationship between the composition of nodules, micronodules, sediments, and pore waters for the areas is given elsewhere (Stoffers et al., 1981).

Briefly, each of the study areas lies beneath the belt of equatorial high productivity in the central Pacific (Figure 1). Significant differences in sedimentation characteristics between the areas are, however, apparent. Although sediment characteristics in each area are locally dependent on topography (water depth), the principal facies encountered in each region can be summarized as follows:

Area *C* at 11°30′ N is a zone of siliceous ooze between the Clarion and Clipperton Fracture Zones. This area is characterized by the presence of lower Miocene sediments approximately 1.2 m beneath the sediment surface; this reflects either a very slow sedimentation rate or intensive erosion by bottom currents since the lower Miocene (cf. Piper et al., 1979b; Frazer and Fisk, 1981). Van Andel et al. (1975, p. 79) have shown that the southern erosional boundary in this region corresponds to the Clipperton Fracture Zone. The migration of Pacific Bottom Water has been documented by Edmond et al. (1971).

Area *D* at 4° N is a zone of calcareous ooze where nodules are absent.

Area *F* at 7° S is a zone of siliceous debris-rich calcareous ooze.

Area *G* at 10° S is a zone of siliceous debris-rich calcareous ooze. This area is tectonically active and the main graben of the Marquesas Fracture Zone runs through the area at about 10° S.

In terms of bathymetry, areas *F* and *G* are characterized by the presence of well-defined seamounts whereas area *C* has a more subdued topography. Schematic maps showing the bathymetry and sample locations of these areas are given in Figures 2–4. Van Andel et al. (1975) have mapped the surface water productivity, carbonate content of Holocene sediments, opal distribution of Holocene sediments, and $CaCO_3$ and residual sedimentation rates in the equatorial Pacific and this publication provides an excellent background of the sedimentological characteristics of the three areas (cf. Figs 1, 4, 5, 38, and 39 of van Andel et al., 1975). A sediment isopach map for

the Pacific has been compiled by Ludwig and Houtz (1979); it shows the much thinner sediment cover at area *C* compared with *F* and *G*. Berger et al. (1976) have also presented a map of the carbonate distribution of the Pacific which includes the study areas. Bischoff and Piper (1979) provide an account of the various factors controlling nodule genesis in the equatorial Pacific; these include bottom current measurements, productivity and faunal studies,

Figure 1. Schematic map showing the locations of the four study areas.

Figure 2. A schematic map showing the bathymetry and station locations in 1 area *C*. Depths in meters. Positioning by satellite fixes and dead reckoning.

sedimentation rates and stratigraphy (including the thickness of the acoustically transparent layer) and effects of sediment redistribution on a local scale. Mizuno et al. (1980) have discussed the role of bottom currents on nodule formation in the Central Pacific Basin. Such factors are beyond the scope of this paper. One of the few previous attempts to study sediment distributions on an equatorial Pacific transect is described by Arrhenius (1952).

Chemical analysis was carried out in samples dried at 105°C for 72 hours using methods identical (XRF and AAS) to those described by Thijssen et al. (1981) for Peru Basin nodules. Because of the large number of samples analyzed in the course of this study (237 samples analyzed for 12 elements), the analytical data are presented in an Appendix for convenience.

During this investigation, it was established that marked mineralogical changes occur when the nodules are heated to 105°C and a phase conversion of todorokite to δ - MnO_2 takes place. Because of this, X-ray diffraction analysis was carried out on samples stored
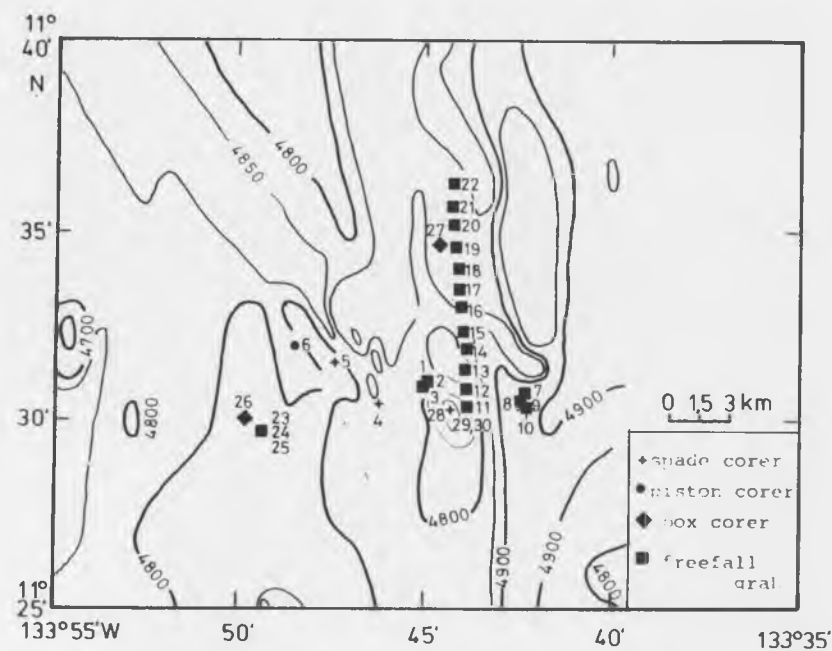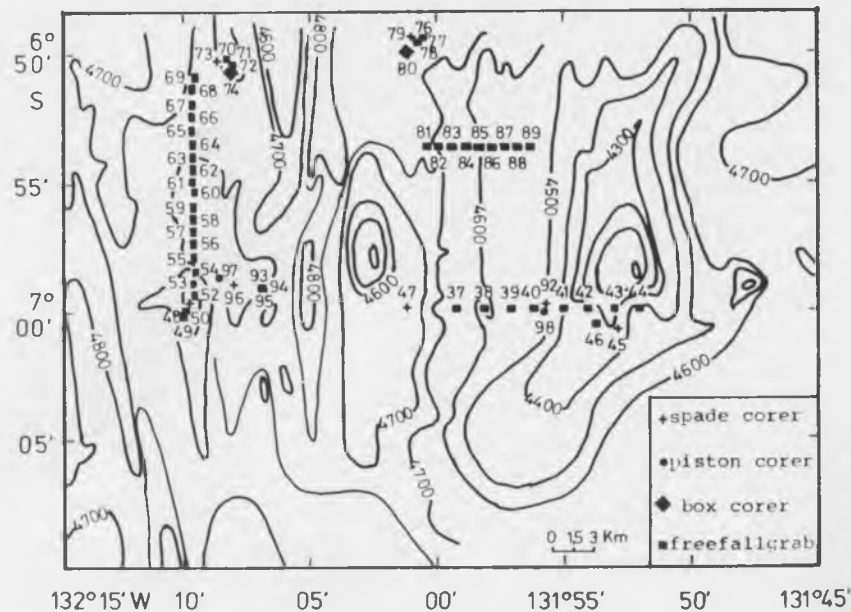

Figure 3. Schematic map showing the bathymetry and station locations in area F. Depths in meters. Positioning by satellite fixes and dead reckoning.
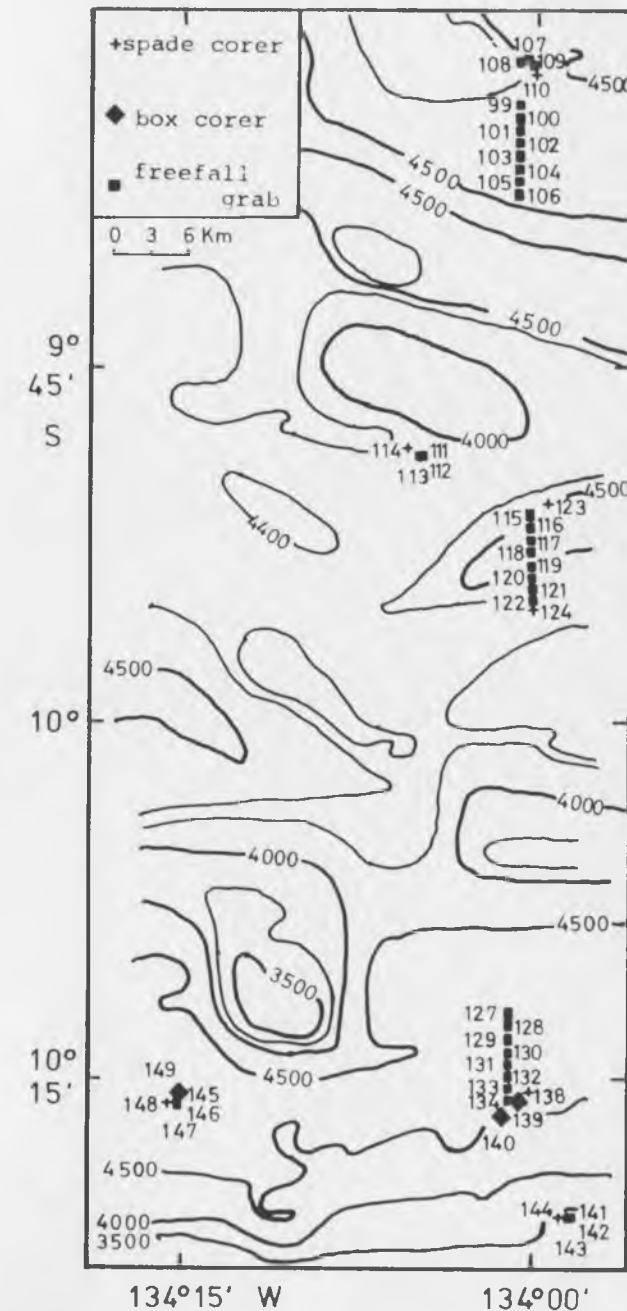

Figure 4. Schematic map showing the bathymetry and station locations in area G. Depths in meters. Positioning by satellite fixes and dead reckoning.

moist in plastic bags (again according to the method of Thijssen et al., 1981). The samples selected for mineralogical analysis were therefore not identical to those chemically analyzed.

Area C

Nodule Morphology

In terms of size, there is a bimodal distribution of nodules with 65% of the nodules occurring in the 0–10 mm size classes and 29% in the size classes greater than 60 mm (Table 1). Only 6% of the nodules occur in the size class 40–60 mm. This suggests that there are two discrete nodule populations present in area C; those less than 40 mm and those greater than 60 mm. These correspond to the younger or "immature" deposit and older or "mature" deposit, respectively, as defined by Craig and Andrews (1978). In terms of nodule weight, however, 92% of the nodules are present in nodules greater than 60 mm and only 5.6% in nodules less than 40 mm. Nodules in the size classes greater than 60 mm are therefore dominant and this factor must be taken into account in any consideration of the overall mass balance of manganese nodule formation in this area; nodules less than 40 mm are of only minor significance in this equation. The average nodule weights in each size class are significantly lower than those determined by Craig (1979) but this may reflect the actual size distribution of nodules in each size class rather than any difference in the density of nodular material. The average weight of nodules from area C is 92.6 g; this is an order of magnitude higher than the corresponding figure for Aitutaki Passage nodules in the Southwest Pacific.

Between individual locations, there are significant differences in the size distribution of the nodules; nodules less than 40 mm in size are much more abundant at location (Loc) 1 (84.2%) and Loc 2 (81.0%) than at Loc 4 (40.6%) and Loc 3 (60.1%). Correspondingly, nodules in the classes greater than 60 mm are much more abundant at Loc 4 (56.2%) and Loc 3 (40.0%) than at Loc 1 (15.8%) and Loc 2 (5.2%). This suggests a fundamental difference in the absolute

Table 1
Summary of abundance of nodules by number and weight and the average nodule weight in each area from each of the study areas.

Size Fraction (mm)	Area C No.	%	Wt. (g)	%	Average nod. wt. (g)	Area F No.	%	Wt. (g)	%	Average nod. wt. (g)	Area G No.	%	Wt. (g)	%	Average nod. wt. (g)	Average nod. wt. (g) (Craig 1979)
0–20	44	26	92	0.6	2.1	3,420	95	4,425	51	1.3	5,069	88.0	7,375	51	1.4	4.0
20–40	66	39	723	5	10.9	163	5	1,386	16	8.5	638	11.0	5,315	37	8.3	20.0
40–60	10	6	455	3	45.5	19	0.5	830	10	43.6	47	0.8	1,410	10	30.0	78.0
60–80	17	10	2,170	14	115	7	0.2	1,000	12	143	2	0.03	300	2	150	242.0
>80	32	19	12,180	78	381	3	0.1	1,030	12	343	–	–	–	–	–	553.0
Total	169		15,620		92.6	3,602		8,671		2.4	5,758		14,400		2.5	

abundance of the two nodule populations between these locations.

Within individual locations, there are significant variations in the nodule size distribution but these may reflect in part the statistical problems of sampling a scattered nodule population displaying a bimodal size distribution with samplers of limited area as well as actual localized variations in size distribution. In terms of nodule shape and surface texture, this is determined principally by nodule size and can be summarized as follows:

0–20 mm: Faceted spheroidal to ellipsoidal nodules with uniform surface texture ranging from smooth to botryoidal.

20–40 mm: Spheroidal or spheroidal-ellipsoidal nodules with suppressed equatorial rims. Surface textures of nodules vary. Some nodules show mammillated smooth surface texture on one side and microbotryoidal on the other. Others show botryoidal surface texture on one side, granular on the other.

40–60 mm: Spheroidal-discoidal to discoidal nodules with equatorial rims; mammillated smooth surface texture on one side; microbotryoidal on the other.

60–80 mm: Discoidal to discoidal-ellipsoidal nodules with equatorial rims; mammillated smooth to microbotryoidal surface texture on one side; microbotryoidal to cavernous botryoidal on the other.

>80 mm: Discoidal-ellipsoidal nodules with equatorial rims; mammillated smooth to microbotryoidal surface texture on one side and mammillated microbotryoidal to botryoidal or cavernous granular surface texture on the other.

A photograph showing the recovered and in situ distribution of nodules at one station is given in Figure 5.

Sediment and biological tubes were often noted to be embedded in the coarser surfaces of the nodules and occasionally a shark's tooth or whale's earbone was noted as nodule nucleus (Figure 6). One nodule at Station (Stn) 7 had a shark's tooth with minimal manganese coating embedded in the smooth surface of the nodule. Thin slivers of volcanic rock with a thin coating of manganese oxides were recovered at Stn 1 and a piece of pumice at Stn 23. At Stn 26 (Loc 3), an irregular discoidal nodule (>80 mm) with a subdued equatorial
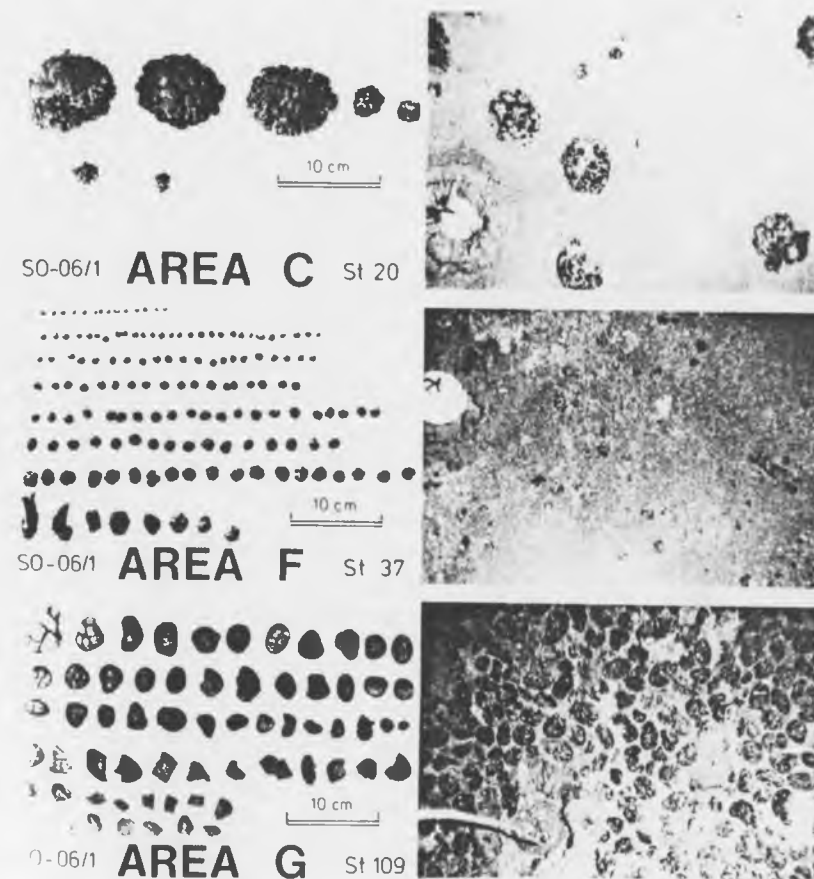
Figure 5. Photographs showing the recovered and in situ distribution of manganese nodules taken by free-fall grab samplers at Stn 20 GB area *C*, Stn 37 GB area *F*, and Stn 109 GB area *G*. The photographed area is somewhat larger than the sampled area. The free-fall grab area is 0.35 m × 0.38 m.

rim was recovered at a depth of 1 m in the sediment by box corer; the surface was mammillated botryoidal heavily embedded with sediment. The outer layer of the nodule could be easily removed to reveal a lustrous, black, smooth, mammillated layer. This was the only buried large nodule found at area *C*.

From the above morphological descriptions, it is seen that there is an almost systematic change in the characteristics of the nodule with increasing size. The shape changes from slightly distorted spheroidal in the size range 0–20 mm, through spheroidal-discoidal (20–60 mm) to discoidal-ellipsoidal nodules (>60 mm). There is therefore a progressive flattening of the nodule shape with increasing size (cf. Raab, 1972). The presence of equatorial rims becomes noticeable in nodules 20–40 mm and pronounced in nodules that are >40 mm. Surface texture is uniform in the small nodules (0–20 mm) but differs on the upper and lower surfaces of the nodules that are >20 mm; the difference in surface-textural characteristics increases with increasing nodule size until, by the largest nodule sizes (>80 mm), there is a marked difference between mammillated microbotryoidal-botryoidal surface texture on one side and the cavernous granular surface texture on the other. In the larger nodules (>60 mm), there is also a difference in the degree of sphericity of the upper and lower surfaces of the nodules. The upper surfaces of the nodules are frequently less concave than those of the undersurfaces, which suggests that the underside accretes at a faster rate (perhaps by a factor of two) (from pore water) than the upper surface (from seawater) at least in the equatorial North Pacific and that the nodule is more deeply embedded in the sediment than it otherwise would be. This faster rate of deposition of authigenic elements on the underside of the nodules presumably reflects the influence of diagenetic processes taking place within the sediment column; it has long been supposed that the high Ni, Cu, and, to a lesser extent, Mn contents of nodules from this "economic grade" nodule zone in the equatorial North Pacific is due to the release of these metals as a result of the decomposition of siliceous frustules within the sediment column. This would also be in agreement with the higher contents of Ni, Cu, and Mn on the underside of these nodules (see section on composition). The higher growth rate in the underside of equatorial North Pacific nodules has now been con-

Figure 6. Photographs of a medium (40–60 mm) discoidal nodule with equatorial rim from Stn 23 GB area *C* showing a whale's earbone as the nodule nucleus.

firmed by Moore et al. (1981). From a study of the bottom photographs taken in area C (see pp. 183-184), it is extremely difficult to establish the precise relationship of the equatorial rim of the nodules to the in situ position of the nodules at the sediment-water interface; this problem awaits further study (cf. Sorem et al. 1979; Felix, 1980). The pronounced mammillated or cavernous structure of the surfaces of the larger nodules suggests that the manganese best accretes in mammillae (up to 15 mm in diameter) rather than on larger uniform flat surfaces.

All these features point to the importance of the rolling characteristics of the nodules on the seafloor in determining the external morphology of the nodules as proposed by Glasby (1977). The smaller nodules are more mobile on the seafloor and therefore become rounded with uniform surface texture. With increasing size, the mobility of the nodules decreases. The nodules therefore become static at the sediment-water interface, develop equatorial rims, different surface textures on upper and lower surfaces (indicative of deposition from sea water and pore water, respectively), and have different degrees of sphericity on the upper and lower surfaces (indicative of differing rates of growth from sea water and pore water). Our evidence (see also Raab, 1972; Dugolinsky, 1976; Sorem and Banning, 1976) indicates that the smoother surface textures generally constitute the upper surfaces of the nodules. This observation is in accord with the findings of Heye (1975) that larger growth cusp patterns of nodules are often indicative of faster growth rates; thus the coarser surface texture on the underside of the nodule is also a reflection of faster growth rates as previously deduced from the sphericity of nodule surfaces. Interestingly, Heath in 1979 suggested that the burial rate of nodules on the seafloor is independent of nodule size and attempted to prove this by demonstrating a linear relationship between the frequency distribution of nodules and size at a given location (Heath, 1979, Figure 1). Such a relationship cannot hold at area C where there is a bimodal distribution of nodules and this hypothesis does not agree with influence of nodule size on the rolling characteristics deduced here. The morphology of the nodule is, of course, also controlled by the characteristics of the nuclei of the nodules; Craig and Andrews (1978) have already differentiated small "immature" and large "ma-

ture" nodules from the equatorial North Pacific on these grounds and the bimodal size distribution of the nodules would support this contention (sea above).

It should be noted that the above approach in which the morphology of the nodules is related to nodule size is fundamentally different from that adopted by Karas and Greenslate (1979) (cf., Mizuno, 1981). By failing to take into account the variations in shape of the nodules with size and the reasons for this, these authors introduced a fundamental error into their models for nodule growth.

Surface Density and Biological Activity

The observed surface densities of nodules (Table 2) confirm Craig's (1979) observation of large-scale local variations in nodule density for the equatorial North Pacific and are somewhat larger than those recorded by him. For example, at Loc 1 and Loc 2, there is an 11–12-fold variation in nodule density over distances of less than 1 km and at Loc 4 a variation from 0–14.3 kg/m² over a distance of 11 km. These variations cannot be attributed to variations in water depth (topography) at Locs 1 and 2 where the depth range is less than 10 m or at Loc 4 where there is no systematic variation in nodule density with water depth. The total depth range for these four locations is 170 m, which is too small for any systematic variation in nodule density with depth to be observed, although there is a minimum between 4,800–4,900 m (Figure 7). It should be noted, however, that Craig's (1979) data for equatorial North Pacific nodules show no systematic variation in the surface density of nodules with water depth as shown by the fact that the highest density of nodules (14.3 kg/m²) occurs at the shallowest water depth (approx 4,250 m at free-fall grab (F.F.G.)/ VA - 17 /B) and the lowest density (0.18 kg/m²) at the greatest depth (approx. 4,960 m at F.F.G. VA - 6). This erratic distribution of density is well illustrated in Figure 7. Care must therefore be taken in interpreting the distribution of nodule densities with water depth. Average surface density at each location in area C is not particularly high with a maximum at 2.1 kg/m² at Loc 4.

Table 2
Average size distribution and surface density of nodules and range of water depths at each location in area *C*.

Size Fraction (mm)	Loc 1 (Stns 1–3)		Loc 2 (Stns 1 7–10)		Loc 4 (Stns 11–22)		Loc 3 (Stns 23–26)		Loc 5 (Stn 27)		Loc 6 (Stn 28)	
	No. / %		No. %		No. %		No. %		No. %		No. %	
0–20	8	42	15	26	11	17	10	29	-	-	-	-
20–40	8	42	32	55	15	23	11	31	-	-	-	-
40–60	-	-	8	14	2	3	-	-	-	-	-	-
60–80	1	5	3	5	12	19	1	3	-	-	-	-
> 80	2	10	-	-	24	37	13	37	-	-	-	-
Total	19		58		64		35					
Average density (kg/m²)	2.8		3.0		7.1		6.5		-		-	
Range of density (kg/m²)	0.6–6.8		0.4–5.6		0.0–14.3		5.0–8.3		-		-	
Water depths (m)	4,825–4,835		4,911–4,916		4,746–4,891		4,779–4,789		4,881		4,656	

Figure 7. Graph showing the variation of the average surface density of manganese nodules from areas *C*, *F* and *G* with water depth at 100-meter intervals. The density data of Craig (1979) for manganese nodules from the equatorial Pacific based on Valdivia VA–09 material is shown for comparison.

An interesting problem that arose in assessing the in situ abundance of nodules from bottom photographs is the apparent discrepancy between the abundance of nodules in the bottom photographs taken from the free-fall grab on contact with the seafloor and the on-board photographs of the nodules recovered from that grab. Often there are wide disparities in nodule distribution in what should be identical areas (Figure 8). Nodules are often recovered from areas which seem, from the bottom photographs, to be devoid of nodules. From such a comparison, it would appear that even some of the larger nodules in area *C* are buried within the sediment and not visible. Most nodules are indeed covered by a thin layer of sediment on the upper surface, particularly in the depressions between mammillae (Figure 5), similar to that previously described by Paul (1976) (cf. Dudley, 1979). The properties of the boundary layer in which manganese nodules occur has recently been discussed by Halbach and Ozkara (1979) and Sorem et al. (1979).

Evidence on biological activity is common. Animals are commonly observed in bottom photographs and include holothurians, sponges, echinoderms, and worms, as well as free-swimming forms such as shrimplike crustaceans and squidlike animals. The animals are more common in areas of higher nodule coverage. Faecal trails and burrowing and mound structures are also observed. Where burrowing or mound building is most common, the nodules appear to have been pushed aside by activity rather than buried by it. This results in somewhat artificial appearing rows of nodules arrayed between or around mounds. Where large mounds (— 1 m) are observed, nodules are scarce and possibly buried.

Composition

Area *C* nodules are characterized by high Mn:Fe ratios (average 5.4) and high Ni and Cu contents (average Ni + Cu, 2.48%) (Table 3) which may be considered to be economic grade. Some differences in composition are apparent between stations at individual locations and between locations but these are not particularly well defined (Table 4) and there appears to be no systematic relationship between nodule composition and topography (cf. Loc 4). In general, the Ni content of the nodules exceeds the Cu content, although
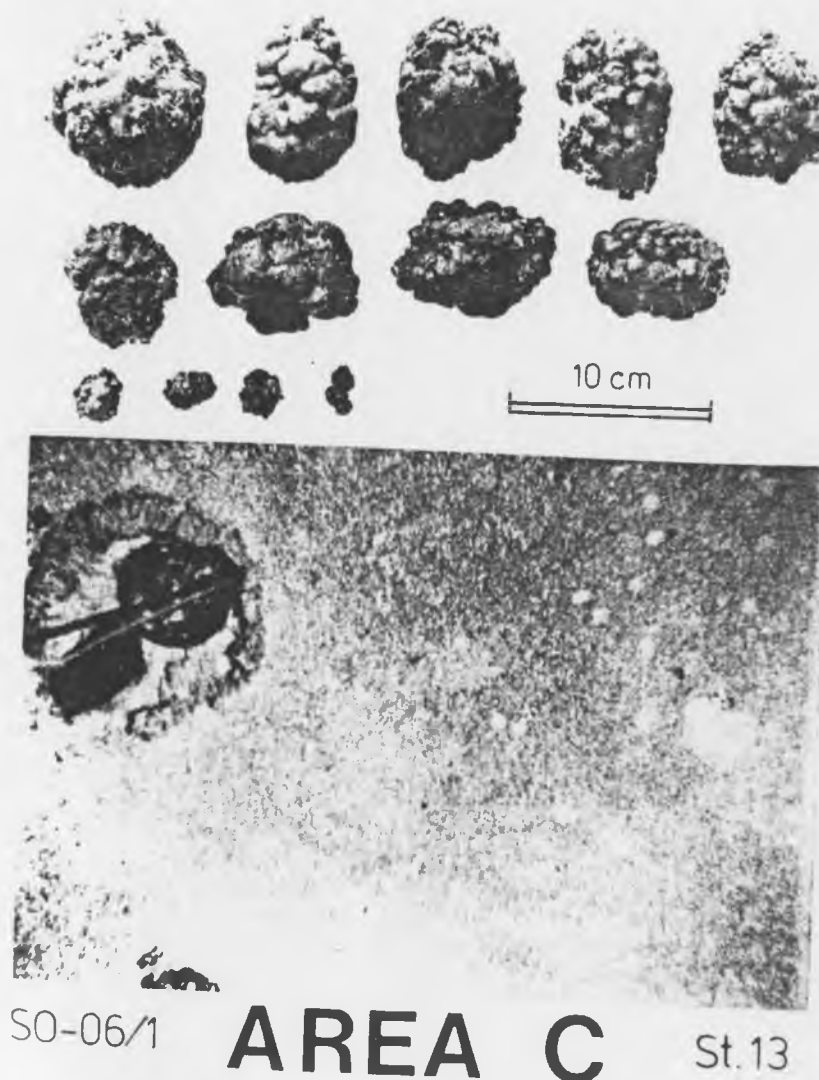
Figure 8. Photographs showed the recovered and in situ distribution of manganese nodules taken by free-fall grab sampler at Stn 13 GB area C.

this is not always so. Ni, Cu, SiO_2, and Al_2O_3 show a tendency to decrease and Fe and U to increase with increasing nodule size but this is not always apparent and many elements remain roughly constant (Table 5). The decrease in silicate content of the nodules with increasing size indicates that the larger nodules do not have a large silicate core. Although these average values are somewhat suspect as the analyzed nodules in each size class are derived from different stations and there is a considerable spread of element concentrations within each size class, these data do show that for the economic elements the large nodules (>60 mm) differ significantly from the smaller nodules (<40 mm) only in the concentration of Ni and Cu which are lower in the larger nodules. Mn, Fe, Co, and Zn show no systematic trends. The two nodule populations can therefore be differentiated compositionally only in terms of their Ni and Cu contents. These findings differ from those of Craig and Andrews (1978) who suggested that larger nodules have higher Mn:Fe ratios and Cu contents than the smaller nodules and of Heye (1979) who suggested that Mn, Ni, and Cu increase slightly with nodule size. Heye was, however, dealing with nodules in the vicinity of a seamount and may therefore have been dealing with a mixed population of seamount and abyssal nodules.

As Raab (1972) has previously shown, the highest contents of Ni, Cu, Zn, and Mn in equatorial North Pacific nodules are found on the underside of the nodules (i.e., in that part in contact with the sediment); this finding suggests that the smaller nodules (0–20 mm) recovered here (which are richer in Ni and Cu) are formed dominantly within the sediment rather than by direct deposition from seawater. The analyses here do, however, represent bulk analyses. These variations in composition with nodule size make no allowance therefore for the influence of variations in nucleus size of the nodules (i.e., proportion of lithogenous phase) on nodule composition. The fact that SiO_2 and Al_2O_3 decrease and Fe and Co increase with increasing nodule size would, however, suggest that the above conclusion is correct and that we are not merely observing dilution of the authigenic elements (Ni, Cu, Zn, and Mn) by silicate material. Analysis of the outer zones, inner zones, and cores of three large nodules from Stns 21, 22, and 25 (cf. Appendix) shows no evidence of Mn, Ni, and Cu depletion and SiO_2 and Al_2O_3 enrichment in the

Table 3

Average composition of nodules from different locations in area C. All analyses in percent, except where otherwise stated.

Location	Station No.	No. of analyses	Mn	Fe	Co	Ni	Cu	Zn	Ba	SiO₂	Al₂O₃	U ppm	Ce ppm	La ppm
1	1–3	6	29.6	4.5	0.22	1.33	1.38	0.17	0.36	16.2	5.8	3.13	231	99
2	7–10	9	26.9	5.8	0.25	1.32	1.12	0.15	0.29	18.0	6.7	3.27	243	108
3	23–26	7	30.1	5.5	0.22	1.27	1.14	0.16	0.37	15.3	5.8	3.34	279	107
4	13–22	18	29.8	5.7	0.22	1.23	1.10	0.16	0.30	14.7	5.6	3.55	283	106
Average		40	29.1	5.4	0.23	1.29	1.19	0.16	0.33	16.1	6.0	3.32	259	105

Table 4

Average chemical composition of nodules at each station from area C. All analyses in percent.

Loc	Stn	Mn	Fe	Co	Ni	Cu	Zn
1	1	31.1	3.6	0.23	1.36	1.50	0.17
	2	29.2	4.8	0.23	1.36	1.49	0.16
	3	28.6	5.1	0.21	1.26	1.16	0.18
2	7	27.8	5.8	0.26	1.29	1.18	0.16
	8	27.2	5.7	0.24	1.30	1.07	0.16
	10	25.6	5.9	0.25	1.38	1.12	0.13
4	13	28.5	4.6	0.20	1.35	1.29	0.15
	14	31.5	6.3	0.24	1.03	0.94	0.15
	15	28.4	6.3	0.23	1.15	0.99	0.14
	16	32.2	5.7	0.24	1.12	1.01	0.18
	18	28.8	6.5	0.22	1.17	1.01	0.15
	19	30.0	5.5	0.23	1.29	1.12	0.16
	20	28.1	4.8	0.22	1.39	1.29	0.17
	21	31.5	5.4	0.19	1.33	1.19	0.17
	22	29.2	6.0	0.21	1.30	1.06	0.16
3	23	31.4	4.7	0.26	1.36	1.39	0.15
	24	29.2	6.0	0.21	1.31	1.10	0.16
	25	31.1	5.4	0.21	1.12	1.00	0.15
	26	28.8	5.7	0.19	1.28	1.05	0.16
Range		25.6–32.2	3.6–6.5	0.19–0.26	1.03–1.39	0.94–1.50	0.13–0.18
Variability (%)		25.8	80.6	36.8	35.0	59.6	38.5

nodule cores relative to the outer zones of the nodules. This clearly demonstrates that the cores of the larger nodules are composed predominantly of manganese oxides, similar in composition to those found in the outer nodule layers, and not of silicate minerals. The cores tend to have high Ba contents which may reflect the presence of barite (see below).

In terms of variability of element composition, the following ranges of element values are observed between stations: Mn, 25.6–32.2%; Fe, 3.6–6.5%; Co, 0.19–0.26%; Ni, 1.03–1.39%; Cu, 0.94–1.50%; Zn, 0.13–0.18%; Ba, 0.27–0.44%; SiO_2, 13.1–20.8%; Al_2O_3, 4.9–7.6%; U, 2.67–4.22 p.p.m.; Ce, 187–330 p.p.m. and La, 80–120 p.p.m. Fe shows the greatest percentage variability in nodule composition between stations (Table 4) as noted by Craig (1979) but there is no evidence for the low variability of Ni or the high variability of Co as reported by that author. The plot of average

Table 5

Mean analyses of nodules by size class in area C. All analyses in percent, except where otherwise stated.

Size Fraction (mm)	No. of analyses	Mn	Fe	Co	Ni	Cu	Zn	Ba	SiO₂	Al₂O₃	U ppm	Ce ppm	La ppm
0–20	3	28.2	5.4	0.24	1.34	1.27	0.15	0.30	18.6	6.6	2.96	223	90
20–40	13	31.4	4.6	0.23	1.42	1.40	0.16	0.31	17.0	6.1	3.22	304	100
40–60	3	27.5	6.0	0.24	1.29	1.04	0.15	0.32	16.4	6.2	3.47	257	117
60–80	6	29.5	5.3	0.22	1.26	1.14	0.15	0.39	14.7	5.5	3.53	285	110
>80	13	28.3	6.1	0.22	1.19	1.00	0.16	0.34	14.8	5.7	3.48	300	108

nodule weight (total wet weight of nodule samples divided by the number of nodules) against Mn:Fe ratios for each station which was used by Craig (1979) to establish "geochemical environments represented at the extremes by hydrothermal-type and hydrogenous-type setting" is not particularly useful for area C (Figure 9) because the principal difference between the nodules from each location is one of size rather than Mn:Fe ratio which has a range of overlapping values.

Mineralogy

X-ray diffraction analysis of four nodules showed todorokite and δ-MnO_2 to be the principal manganese oxide minerals and quartz and probably feldspar and/or zeolite to be the principal silicate minerals present (Table 6). From the relative intensities of the peaks, it was concluded that both todorokite and δ-MnO_2 were present and it was not possible to distinguish feldspar and zeolite in the nodules by this method. The underlined minerals in the table represent the principal minerals present. A more detailed study of the mineralogy of equatorial North Pacific nodules has been given by Sorem and Fewkes (1980).

Area F

Nodule Morphology

In terms of size, nodules are mostly small, 95% being in the size range 0–20 mm and less than 1% being in the size range greater than 40 mm (Table 1). Although there is a continuous spectrum of nodule sizes throughout the entire size range, a significant proportion of the nodules is extremely small, of the order of 5 mm in diameter. This is reflected in the low average weight of nodules in the 0–20 mm size class (1.3 g) and indeed the low overall average weight of nodules from this area (2.4 g). The size distribution of the nodules suggests that they represent one population. In spite of the paucity of nodules in the size classes greater than 40 mm (< 1%), these nodules make up 34% of the total weight of nodules in this area.
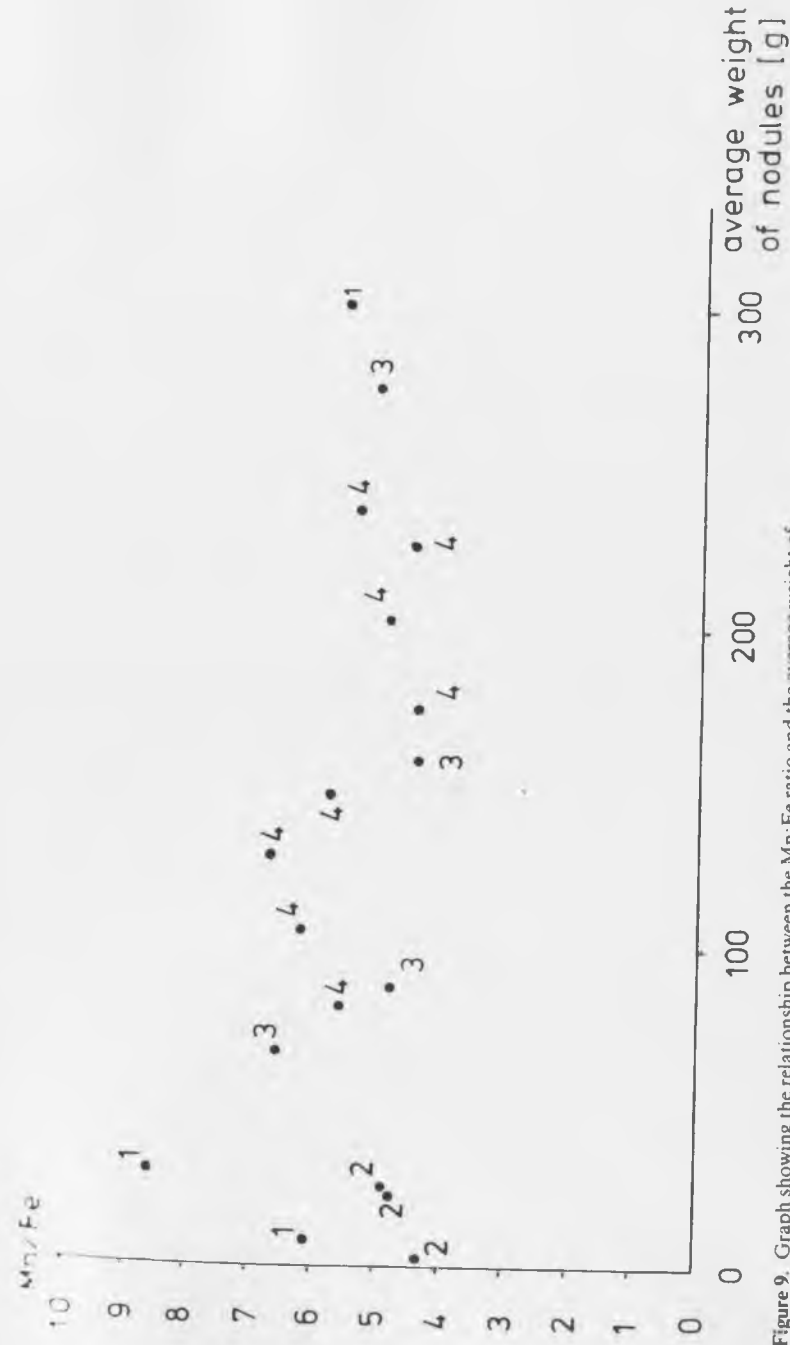

Figure 9. Graph showing the relationship between the Mn:Fe ratio and the average weight of nodules from each station at area C following the method of Craig (1979). The numbers represent location numbers.

Table 6

X-ray diffraction analysis of nodules from area *C*. The principal mineral phases present are underlined.

Stn	Size Fraction (mm)	Definite	Probable
7 GB	20–40	Todorokite, δ-MnO₂ Quartz, Illite	Feldspar and/or Zeolite •
10 KG	broken nodule	Todorokite, δ-MnO₂ Quartz, Illite	Feldspar and/or Zeolite
18 GB	0–20	Todorokite, δ-MnO₂ Quartz	Feldspar and/or Zeolite
23 GB	0–20	Todorokite, δ-MnO₂ Quartz,	Feldspar and/or Zeolite

There are variations in nodule distribution between individual locations. At Locs 9 and 10, there are higher proportions of nodules in the size classes greater than 20 mm (18–24%) than at other locations (2–9%). Higher abundance of larger nodules may therefore be related to water depth (i.e., the carbonate compensation depth, C.C.D.) since Locs 9 and 10 are the two deepest stations; the lower sedimentation rate would presumably favor the growth of larger nodules. This is confirmed by a study of the size distribution of the nodules with depth which shows a marked increase in proportion of nodules in the size classes greater than 20 mm at depth greater than 4,700 m. Between stations at a given location, there are differences in the relative abundances of the larger nodules but again the statistical problems of sampling the relatively scattered populations of larger nodules (> 20 mm) become apparent.

Nodule shape and surface texture are again determined principally by nodule size. The larger proportion of nodules in the 0–20 mm size class, however, ensures that the morphology of these small nodules dominates. Briefly, the nodule morphologies can be summarized as follows:

0–20 mm: Spheroidal nodules with botryoidal, or more rarely, smooth surface texture. Limited number of polynucleate nodules and manganese-encrusted sharks' teeth.

20–40 mm: Ellipsoidal to spheroidal nodules with botryoidal or, more rarely, microbotryoidal or smooth surface texture. Occa-

sional cylindrical or discoidal nodules. Limited number of polynucleate nodules and manganese-encrusted sharks' teeth.

40–60 mm: Ellipsoidal to discoidal nodules mostly with equatorial rims. Surface texture ranges from botryoidal in some nodules to smooth surface texture on one side and microbotryoidal on the other in other nodules. Some surfaces are mammillated or cavernous.

60–80 mm: Discoidal to ellipsoidal nodules with equatorial rims; botryoidal to cavernous botryoidal surface texture.

>80 mm: Discoidal to tabular-discoidal nodules with equatorial rims, one spheroidal nodule. Surface texture ranges from cavernous botryoidal to microbotryoidal surface texture. One nodule has mammillated smooth surface texture on one side and botryoidal on the other.

A photograph showing the recovered and in situ distribution of nodules at one station is given in Figure 5.

Volcanic rock was also recovered at Stn 54 (Loc 10), 92 (Loc 8), and 93 (Loc 15). At Stn 54, this consists of a large quantity of fragmented, angular, relatively unweathered volcanic rock coated with a thin but variable thickness of manganese. In many cases, the manganese has developed an equatorial rim at the in situ sediment-water interface. In the case of the larger rock material, one sample had only a thin veneer of manganese, whereas another of comparable size had a thick (15 mm) manganese coating on one side of the rock material while the other (probably under) side was devoid of manganese. The manganese in this sample has a smooth to microbotryoidal surface texture becoming botryoidal at the equatorial rim. In the case of the smaller samples, the volcanic rock had been almost completely replaced by manganese. At Stns 92 and 93, the material was angular, relatively unweathered volcanic rock with a thin coating of manganese. At Stns 54 and 93, the volcanic rock was found together with nodules. At Stn 94, irregular manganese encrustations were found. Biological tubes could be seen in the surface of many nodules mainly between botryoids.

The above-noted changes in nodule morphology with size are therefore analogous to those observed in area *C*, although some differences are encountered, particularly in the surface texture of the nodules. At area *F* though, the smaller nodules predominate.

Surface Density and Biological Activity

Because of the small average size of the nodules, nodule densities are low and they vary from 0.2 to 2.6 kg/m² (between locations) on the average (Table 7). There is considerable variation in density both between stations within a given location and between locations. Locs 12, 13, and 15 have the highest nodule densities (average 2.2–2.6 kg/m²), possibly because the stations are clustered in depressions. At one location (Loc 10), the nodule distribution varies 50-fold (0.1–5.0 kg/m²) over distance of 9 km. Overall, the nodule density is dependent on the water depth (C.C.D.) as shown in Figure 7 where a sharp increase in nodule density between 4,700 and 4,900 m is observed which then drops at depths greater than 4,900 m. Figure 7 also shows that environmental parameters other than depth are important in controlling the surface densities of nodules at a given location since the surface densities of nodules at a given depth are approximately three to five times lower at area F than at area C. On an individual traverse such as Locs 10–11 (Stns 52–69), however, this depth dependence cannot be so precisely followed. In bottom photographs, the larger nodules at least can be seen widely scattered at the surface of the sediment.

Evidence of biological activity (bioturbation) is again common in area F. In some regions of highest bioturbation, nodules appear to be absent in the bottom photographs but were actually recovered in the free-fall grabs. This suggests that the nodules may be temporarily buried by extensive bioturbation. Many of the exposed nodules are covered by a thin layer of sediment.

Composition

Area F nodules are again characterized by high Mn:Fe ratios (average 4.8) and Ni and Cu contents (average Ni + Cu, 2.54%) (Table 8); the Ni and Cu concentrations are the highest of the three areas studied. In general, the Cu content of the nodules exceeds the Ni content but this is not always so. Although on the basis of grade considerations alone, these nodules are potentially economic, their low surface density would preclude economic exploitation. Variation in nodule composition between stations at individual locations

Table 7

Average size distribution and surface density of nodules and range of water depths at each location in area F.

Size Fraction (mm)	Loc 8 (Stns 37–47,92) No.	%	Loc 9 (Stns 48–51) No.	%	Loc 10 (Stns 52–60) No.	%	Loc 11 (Stns 61–69) No.	%	Loc 12 (Stns 70–75) No.	%	Loc 13 (Stns 76–80) No.	%	Loc 14 (Stns 81–91) No.	%	Loc 15 (Stns 93–98) No.	%
0–20	227	96	26	76	246	80	73	91	914	95	506	98	486	98	1034	97
20–40	7	4	8	24	56	18	3	4	48	5	11	2	6	1	26	2
40–60	-	-	-	-	4	1	2	2	9	0.1	1	0.2	1	0.2	2	0.2
60–80	-	-	-	-	2	0.6	2	2	2	0.02	-	-	1	0.2	-	-
>80	-	-	-	-	-	-	-	-	1	0.01	1	0.2	1	0.2	-	-
Total	234		34		308		80		974		519		495		1062	
Average density (kg/m²)	0.2		0.2		1.2		0.6		2.6		2.2		0.6		2.5	
Range of density (kg/m²)	0.0–1.5		0.0–0.6		0.1–5.0		0.0–4.3		0.3–5.6		0.0–4.1		0.0–2.6		0.0–4.1	
Water depths (m)	4,301–4,682		4,913–4,918		4,761–4,913		4,705–4,853		4,789–4,866		4,750–4,796		4,511–4,759		4,824–4,887	

Table 8

Average composition of nodules from different locations in area F. All analyses in percent, except where otherwise stated.

Location	Station No.	No. of analyses	Mn	Fe	Co	Ni	Cu	Zn	Ba	SiO₂	Al₂O₃	U ppm	Ce ppm	La ppm
8	37	8	30.7	7.7	0.13	1.33	1.35	0.16	0.19	16.3	5.0	3.11	103	88
9	49–50	2	35.5	4.7	0.08	1.22	1.47	0.22	0.26	12.1	4.4	3.68	103	85
10	52–59	23	33.8	6.2	0.11	1.27	1.40	0.18	0.26	13.3	4.5	3.37	110	87
11	61–67	9	32.9	5.4	0.10	1.17	1.32	0.19	0.26	14.9	5.3	3.10	113	86
12	70–75	21	31.8	6.9	0.12	1.12	1.29	0.17	0.23	14.3	4.9	3.27	120	92
13	76–78	14	32.8	6.5	0.12	1.30	1.35	0.18	0.24	14.7	5.0	2.97	114	94
14	81–89	18	29.9	7.5	0.12	1.24	1.29	0.17	0.22	16.6	5.2	3.18	104	94
15	93–95	12	28.9	8.7	0.13	1.18	1.17	0.15	0.19	19.0	5.8	2.88	115	94
Average		107	32.0	6.7	0.11	1.23	1.31	0.18	0.23	15.2	5.0	3.08	110	90

and between locations is apparent, although not particularly marked (Table 9). The composition does not, however, appear to be related to water depth (topography). There is some variation in composition with nodule size (Table 10), although nodules from the size-class 0–20 and 20–40 mm at the same stations generally tend to be very similar in composition, which suggests that they constitute the same nodule population. As for area C, Ni and Cu decrease in concentration with increasing nodule size (Table 10). Ba increases and SiO_2, Al_2O_3, and U decrease with increasing nodule size but there is no systematic trend for the other elements. The following element ranges are observed between stations: Mn, 26.9–35.6%; Fe, 4.6–9.4%; Co, 0.08–0.17%; Ni, 1.11–1.38%; Cu, 1.10–1.52%; Zn, 0.14–0.22%; Ba, 0.18–0.33%; SiO_2, 11.8–21.0%; Al_2O_3, 3.8–6.3%; U, 2.24–3.88 p.p.m.; Ce, 95–148 p.p.m.; and La, 75–120 p.p.m. These indicate that all elements display moderately wide compositional ranges similar to those encountered in area C nodules. Again, the plot of average nodule weight against Mn:Fe ratio of nodules at each station as used by Craig (1979) is not particularly useful (Figure 10) because the principal variation between stations is one of nodule size rather than Mn:Fe ratio. Indeed, there is a considerable overlap of Mn:Fe ratios with those of area C in spite of the markedly different average nodule weight at each station.

Mineralogy

X-ray diffraction analyses of four nodules showed the mineralogy to be similar to that at area C (Table 11). In one sample from Stn 73 KG in the 0–20 mm size class, zeolite is more abundant than the manganese oxides minerals. Unfortunately, no chemical analysis is available for this sample.

Area G

Nodule Morphology

In terms of size, nodules are mostly small, 88% are in the size range 0–20 mm and less than 1% are in the size range greater than 40 mm

Table 9

Average chemical composition of nodules at each station from area *F*. All analyses in percent.

Loc	Stn	Mn	Fe	Co	Ni	Cu	Zn
8	37	30.7	7.7	0.13	1.33	1.35	0.16
9	49	35.3	4.6	0.08	1.25	1.47	0.22
	50	35.6	4.7	0.08	1.18	1.46	0.22
10	52	33.8	6.8	0.12	1.32	1.38	0.17
	53	35.4	5.7	0.11	1.38	1.47	0.19
	54	30.4	9.3	0.15	1.18	1.14	0.14
	55	35.0	4.9	0.09	1.26	1.48	0.21
	57	34.8	4.7	0.09	1.27	1.52	0.21
	59	33.3	5.9	0.10	1.21	1.38	0.18
11	61	33.8	4.7	0.09	1.17	1.45	0.22
	62	35.3	6.6	0.10	1.11	1.20	0.16
	63	30.0	5.9	0.13	1.11	1.10	0.17
	64	33.1	5.0	0.09	1.23	1.42	0.20
	67	32.1	5.0	0.08	1.21	1.45	0.20
12	70	29.1	8.0	0.13	1.24	1.21	0.14
	71	30.6	7.5	0.12	1.31	1.31	0.16
	72	34.4	5.2	0.11	1.29	1.45	0.22
	74	30.7	8.2	0.13	1.24	1.15	0.16
	75	34.0	5.8	0.10	1.16	1.32	0.21
13	76	31.4	7.0	0.12	1.36	1.35	0.17
	77	32.9	6.7	0.13	1.33	1.37	0.16
	78	34.1	5.8	0.10	1.22	1.33	0.20
14	81	32.6	6.3	0.10	1.20	1.36	0.18
	83	32.4	6.2	0.11	1.28	1.38	0.19
	84	27.8	8.7	0.12	1.21	1.22	0.14
	85	31.1	7.3	0.13	1.32	1.34	0.18
	87	28.1	6.7	0.10	1.21	1.28	0.16
	88	30.2	7.3	0.17	1.28	1.31	0.17
	89	26.9	9.4	0.13	1.17	1.16	0.14
15	93	30.1	8.5	0.14	1.21	1.19	0.14
	94	28.4	9.0	0.13	1.17	1.15	0.15
	95	28.2	8.6	0.12	1.17	1.17	0.15
Range		26.9–35.6	4.6–9.4	0.08–0.17	1.11–1.38	1.10–1.52	0.14–0.22
Variability (%)		32.3	104	112	24.3	38.2	57.1

Table 10

Mean analyses of nodules by size class in area *F*. All analyses in percent, except where otherwise stated.

Size Fraction (mm)	No. of analyses	Mn	Fe	Co	Ni	Cu	Zn	Ba	SiO$_2$	Al$_2$O$_3$	U ppm	Ce ppm	La ppm
0–20	55	30.8	7.3	0.12	1.27	1.33	0.17	0.20	16.7	5.3	3.08	108	88
20–40	16	32.2	7.0	0.11	1.24	1.30	0.17	0.23	14.4	4.9	3.24	116	92
40–60	6	33.1	6.8	0.12	1.20	1.27	0.18	0.31	13.0	4.3	3.50	130	82
60–80	6	31.6	6.6	0.11	1.09	1.14	0.17	0.38	13.6	4.4	2.65	104	97
>80	2	31.2	6.9	0.12	1.10	1.09	0.18	0.32	14.5	3.9	2.30	112	105
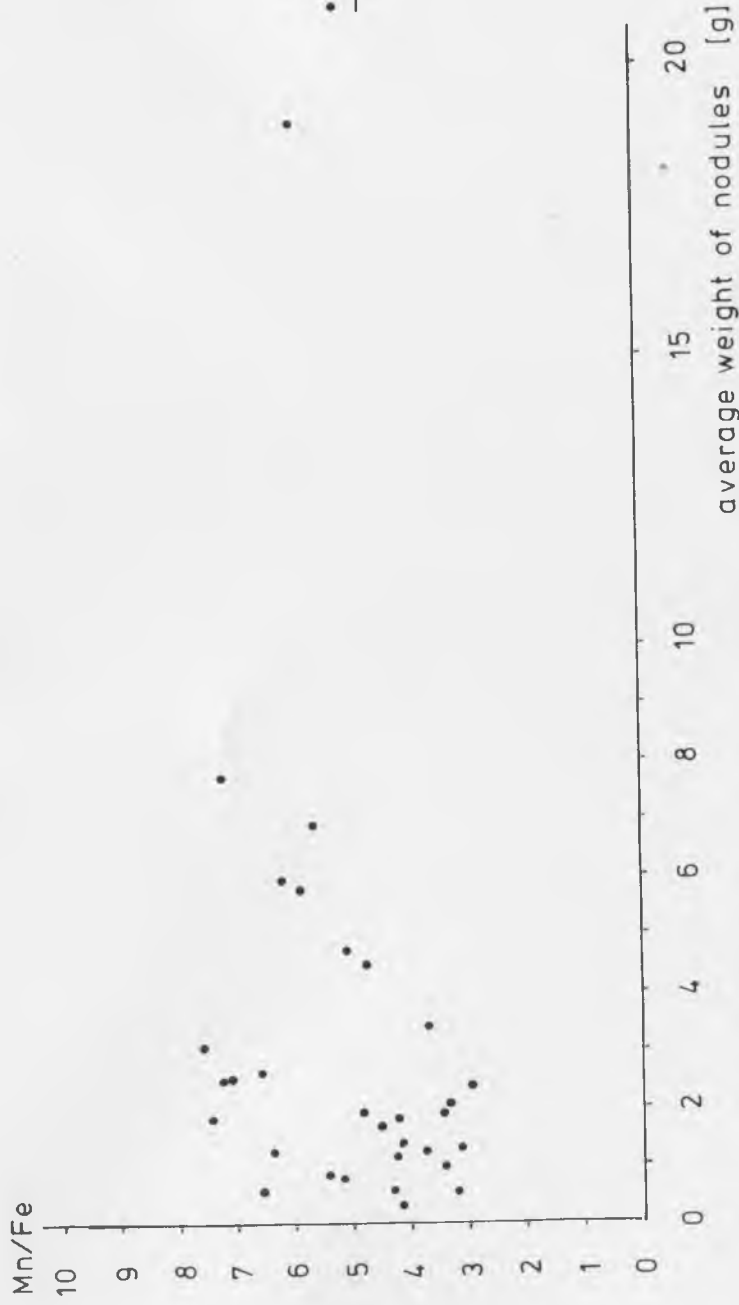
Figure 10. Graph showing the relationship between the Mn:Fe ratio and the average weight of nodules from each station at area F following the method of Craig (1979).

Table 11

X-ray diffraction analysis of nodules from area F. The principal mineral phases present are underlined.

Stn	Size Fraction (mm)	Definite	Probable
53 GB	0–20	Todorokite, δ-MnO$_2$, Quartz	Feldspar/or Zeolite, Illite
63 GB	40–60	Todorokite, δ-MnO$_2$	Quartz
73 KG	0–20	Zeolite, Todorokite, δ-MnO$_2$, Illite	
95 GB	0–20	Todorokite, δ-MnO, Quartz, Illite	Feldspar and/or Illite

(Table 1). Again, the smallest nodules are of the order of 4 mm in diameter. The average weight of nodules in each size class is comparable to that at Area F. The low overall average weight (2.5 g) again reflects the small average size of the recovered nodules.

In terms of the size distribution of nodules, this shows some variation between locations with the lowest proportion of nodules in the 0–20 mm size class being at Loc 17 (76%) and the highest at Loc 23 (99%) (Table 12). In contrast to the situation at area F, the location (Loc 17) with the highest proportion of nodules greater than 20 mm is the shallowest; however, only 33 nodules were recovered at this location and there is no apparent trend in nodule size distribution with depth. Significant variations in the size distribution of nodules between stations at a given location were observed.

Nodule shape and surface texture are more complex than at areas C and F. The commonest nodule type is spheroidal to ellipsoidal with smooth surface texture displaying septuarian cracks. The shape varies with size from predominantly spheroidal in the smallest (0–20 mm) nodules to ellipsoidal (ovoidal) in nodules greater that 20 mm; this transition in nodule shape can take place at about 10 mm nodule diameter at some stations. The tendency of the nodules to display increasing flatness with increasing size is therefore again observed. The ovoidal nodules correspond to the kidney-shaped nodules mentioned by Raab and Meylan (1977). Some of the larger (40–60 mm) nodules are discoidal, sometimes fragmented, with surface texture on one side and microbotryoidal on the other and displaying septuarian cracking. Because of the complexity of nodule morphology in area G, the principal nodule morpholo-

Table 12

Average size distribution and surface density of nodules and range of water depths at each location in area G.

Size Fraction (mm)	Loc 16 (Stns 99–110)		Loc 17 (Stns 111–114)		Loc 18 (Stns 115–125)		Loc 19 (Stn 126)		Loc 20 (Stns 127–136,138,139)		Loc 21 (Stn 137)		Loc 22 (Stns 140–144)		Loc 23 (Stns 145–149)	
	No.	%	No.	%	No.	%	No.	%	No.	%	No.	%	No.	%	No.	%
0–20	838	80	25	76	1,706	86	–	–	1,452	85	–	–	–	–	1,060	99
20–40	99	10	6	18	266	13	–	–	253	15	–	–	–	–	12	1
40–60	31	3	2	6	11	0.6	–	–	3	0.2	–	–	–	–	–	–
60–80	2	0.2	–	–	–	–	–	–	–	–	–	–	–	–	–	–
>80	–	–	–	–	–	–	–	–	–	–	–	–	–	–	–	–
Total	970		33		1,983		No sample (dredge)		1,708		120 kg nodules and crusts (dredge)-sample not sorted		No nodules recovered		1,072	
Average density (kg/m²)	6.1		0.6		6.6		–		2.6		High		0.0		2.3	
Range of density (kg/m²)	0.0–14.7		0.0–2.5		3.7–10.5		–		0.0–6.0		–		–		0.0–3.8	
Water depths (m)	4,522–4,622		4,184–4,189		4,367–4,565		4,570		4,608–4,697		4,453		3,403–4,555		4,687–4,697	

gies at each location at area G are listed in Table 13. Stn 137 (Loc 21) was a dredge haul where a large quantity of manganese crusts was recovered in addition to nodules. For this reason, the material from this station is described more fully than that at other locations. A photograph showing the recovered and in situ distribution of nodules at one station is given in Figure 5.

Three principal features complicate nodule morphology at Area G:

(*1*) The presence of septuarian cracks on the nodule surfaces represent zones of weakness along which the nodule can easily fragment. This has resulted not only in an extensive number of fragmented nodules in situ which can be seen in bottom photographs but has also provided abundant fragmented nodule material that forms a source material for polynucleate nodule formation. In the case of some of the larger nodules, the in situ fragmented nodule surface has been overgrown by further layers of manganese oxides. At many stations, a significant proportion of the nodular material was reported under the heading "fragments"; most of this fragmentation had occurred in situ. Because of the inherent weaknesses in the nodules, however, many more nodules were crushed on transport to Aachen.

Heye (1975) has developed a model for the cracking of nodules due to internal stresses and suggested that "the cracking frequency in nodules offers a good possibility of qualitatively judging the age differences in nodules." However, the difference in fragmentation of nodules at area G and areas C and F results from the presence of septuarian cracks (or lines of weakness) on the nodule surface at area G. Fragmentation of the nodules is therefore dependent not only on the age of the nodule but also on other growth-related parameters (such as septuarian features) which vary with area and whose origins are not yet understood.

(*2*) The presence of relatively fresh angular volcanic rock fragments of varying sizes that are often iron (reddish) or manga-

Table 13
Summary of the principal nodule types found at area G.

Loc	Stn	Morphology
16	99–110	Characteristic spheroidal-to-ellipsoidal (ovoidal or kidney-shaped) nodules displaying smooth surface texture and septuarian features. Variable amounts of fragmented and polynucleate nodules. Polynucleate nodules are most common at Stn 99 where they make up about 30% of the nodule population but are much less common at other stations. Angular volcanic rock fragments at Stn 107.
17	111–114	Similar to above. Mainly mononodules.
18	115–125	Polynucleate nodules predominate at all stations except 119 and 124 where mononodules predominate. Basic nodule type as above. Angular volcanic rock fragments at Stn 115, 116, and 121.
20	127–136, 138, 139	Dominantly polynucleate nodules. Quantity of volcanic rock fragments at most stations. Manganese-encrusted fragments of this volcanic rock have become involved in polynucleate nodule formation. Some of the nodules have fragments of volcanic rock adhering to the nodule surface.
21	137	Dredge haul containing 120 kg of manganese nodules and crusts. There are two populations of nodules: (*1*) Mainly polynucleate with some ovoidal nodules displaying smooth surface texture and septuarian cracks, and (*2*) discoidal nodules with equatorial rims and mammillated microbotryoidal to botryoidal surface texture (one of these nodules has fragmented in situ and manganese has overgrown the fragmented surface). Several types of manganese crust were recovered. *Crust A:* thick (30 mm) black granular manganese crust with granular upper surface and smoother underside. *Crust B:* thick (60 mm) manganese-encrusted basalt. The exposed basalt on the underside is stained reddish brown from iron oxides. *Crust C:* cavernous porous busaltic material covered with a thin layer of manganese oxides. Brownish surface of the weathered basalt exposed in elevated areas. *Crust D:* tabular material (almost nodular) with micro-botryoidal surface texture on one side and cavernous smooth surface texture on the other. Highly altered volcanic core. *Pumice:* one sample of manganese-encrusted pumice.
23	145–149	Dominantly polynucleate nodules. Many small iron-stained angular volcanic rock fragments adhering to the surface of the nodules.

nese (black) stained. Often the iron staining occurs on one side (underside?) of the fragment and the manganese staining on the other. The occurrence of these volcanic fragments is probably related to the proximity of the area to the Marquesas Fracture Zone.

(3) The tendency for polynucleate formation. This can be between whole nodules but the process of polynucleate nodule formation is significantly enhanced by the presence of fragments both of nodules and volcanic rock. Multiple-nuclei polynucleate nodules can form in some cases. In addition to the smaller fragments of volcanic rock participating in polynucleate nodule formation to form irregular polynucleate nodules, very small fragments of this material fleck the surface of some nodules. This feature is much more marked at Loc 20, 21, and 23 than at the other locations.

These three factors (fragmentation, volcanic rock occurrence, and polynucleate nodule formation) occur to markedly different extents between stations and between locations and this results in the more complex morphology at area *G* compared with areas *C* and *F*. For example, the occurrence of volcanic rock fragments and their influence on polynucleate nodule formation is much more marked at Locs 20, 21, and 23 in the vicinity of the seamounts immediately south of the main fault. This shows a clear geological control on the "seeding" of the nodules and therefore on nodule morphology. Other morphological variations are, however, more difficult to interpret. At Loc 18, for example, most stations are characterized by the presence of abundant polynucleate nodules but at Stns 119 and 124 the nodules are dominantly mononucleate. The reason for such localized variations in the relative frequency of mono- and polynucleate nodules is more difficult to ascertain. Again, there appears to be a minimum nodule size of about 4 mm. At some stations, particularly where fragmentation and polynucleate formation is pronounced, there appears to be a continuous size distribution of nodules. Biological tubes were generally absent on smooth nodule surfaces but could be observed on microbotryoidal or botryoidal surfaces where they can adhere to the coarse nodule surface. The occasional shark's tooth was also observed.

Surface Density and Biological Activity

Because of the small average size of the nodules, nodule densities are low and vary between locations from 0.0 to 6.6 kg/m² on average (Table 12). There is a considerable variation in density both between stations within a given location and between locations; the density ranges from 0.0 to 14.7 kg/m² over a distance of 11 km at Loc 16, for example.

Again, nodule density appears to be dependent on water depth as shown in Fig. 7, although the relationship is different from those found at areas C and F. On an individual traverse such as Loc 16, however, there appears to be no precise relationship between nodule density and water depth. Many volcanic rock fragments were recovered at area G, particularly at Locs 20, 21, and 23. These were not included in the computation of nodule density. In bottom photographs, the wide variation in nodule coverage between adjacent stations can be seen and evidence of in situ fracturing of the nodules is relatively common.

Evidence of biological activity (bioturbation) is common in area G and occurs in both nodule-rich and barren areas. At some bioturbated stations, nodules could not be seen in the bottom photograph but were recovered in the free-fall grab; these nodules were, however, usually relatively small. Nodules frequently had some sediment covering on the upper surface.

Composition

Area G nodules are characterized by high Mn:Fe ratios (average 2.2) and high Ni and Cu contents (average Ni + Cu, 1.81%) (Table 14), although these values are lower than those at areas C and F. In general, the Ni content of the nodules exceeds the Cu content. On the basis of grade, area G nodules would not appear to be economic at present. Variation in nodule composition between stations and between locations is generally much greater than that at areas C and F but does not appear to be related to water depth (Table 15). There is some evidence of variation in the composition with size class; nodules in the 40–60 and 60-80 mm sizes show slightly higher Mn, Cu, and Zn and lower Fe contents than those from the

Table 14

Average composition of nodules from different locations in area G. All analyses in percent, except where otherwise stated.

Location Station No.	No. of analyses	Mn	Fe	Co	Ni	Cu	Zn	Ba	SiO₂	Al₂O₃	U ppm	Ce ppm	La ppm
16　99–110	26	33.6	10.8	0.10	1.00	0.94	0.19	0.27	10.4	5.2	3.58	115	99
17　114	4	29.4	12.8	0.12	1.11	0.87	0.15	0.19	14.1	7.1	3.91	125	113
18　115–124	29	28.2	13.7	0.13	1.01	0.79	0.15	0.23	13.5	6.6	4.18	148	116
20　127–138	18	25.2	13.0	0.11	0.92	0.74	0.13	0.21	19.7	8.1	3.57	120	94
21　137	10	29.7	11.9	0.11	1.03	0.88	0.18	0.25	13.8	6.5	3.73	111	83
23　145–147	9	24.0	14.5	0.12	0.91	0.64	0.12	0.17	20.8	8.6	3.59	133	96
Average	96	28.4	12.8	0.12	1.00	0.81	0.15	0.22	15.4	7.0	3.76	125	100

Table 15

Average chemical composition of nodules at each station from area G. All analyses in percent.

Loc	Stn	Mn	Fe	Co	Ni	Cu	Zn
16	99	32.4	11.5	0.13	1.11	1.05	0.17
	100	35.6	10.6	0.10	1.07	1.00	0.20
	101	29.2	14.2	0.11	0.91	0.82	0.16
	102	34.3	6.9	0.07	0.84	0.96	0.24
	107	35.2	8.3	0.07	0.96	1.02	0.22
	108	34.3	11.4	0.11	1.07	0.93	0.18
	109	33.1	11.9	0.12	1.07	0.87	0.18
	110	34.3	11.3	0.11	1.01	0.85	0.19
17	114	29.4	12.8	0.12	1.11	0.87	0.15
18	115	25.6	16.8	0.16	0.82	0.58	0.12
	116	25.4	16.2	0.16	0.84	0.58	0.12
	118	29.2	12.6	0.12	1.12	0.87	0.15
	119	31.2	9.6	0.10	1.14	1.05	0.18
	120	32.5	12.0	0.11	1.10	0.95	0.18
	121	27.7	14.6	0.13	1.06	0.76	0.14
	122	28.0	12.5	0.12	1.16	0.83	0.15
	123	22.1	18.0	0.14	0.72	0.50	0.11
	124	32.3	10.7	0.10	1.05	0.97	0.20
20	127	20.4	12.6	0.10	0.84	0.62	0.11
	128	21.0	13.7	0.11	0.79	0.57	0.10
	130	25.1	15.6	0.13	0.86	0.66	0.13
	131	26.5	13.8	0.13	1.06	0.78	0.14
	132	23.8	13.2	0.11	0.96	0.75	0.12
	133	28.9	9.7	0.09	1.12	1.04	0.17
	138	30.8	12.5	0.11	0.83	0.78	0.16
21	137	29.7	11.9	0.11	1.03	0.88	0.18
23	145	25.5	14.2	0.12	0.91	0.68	0.13
	146	22.6	14.0	0.11	0.92	0.62	0.11
	147	23.9	15.3	0.12	0.91	0.63	0.11
Range		20.4–35.6	6.9–18.0	0.07–0.16	0.72–1.16	0.50–1.05	0.10–0.24
Variability (%)		74.5	161	129	61.1	110	140

size classes less than 40 mm (Table 16). No nodules larger than 80 mm were, however, analyzed. The following total element ranges (excluding the manganese crusts from Stn 137 DK) were observed: Mn, 20.4–35.6%; Fe, 6.9–18.0%; Co, 0.07–0.16%; Ni, 0.72–1.16%; Cu, 0.50–1.05%; Zn, 0.10–0.24%; Ba, 0.15–0.36%; SiO$_2$, 9.7–26.2%; Al$_2$O$_3$, 4.5–10.3%; U, 2.79–4.89 p.p.m.; Ce, 60–220 p.p.m.; and La, n. d.–203 p.p.m. Again, the plot of average nodule

Table 16

Mean analyses of nodules by size class in area G. All analyses in percent, except where otherwise stated.

Size Fraction (mm)	No. of analyses	Mn	Fe	Co	Ni	Cu	Zn	Ba	SiO$_2$	Al$_2$O$_3$	U ppm	Ce ppm	La ppm
0–20	46	27.6	12.8	0.12	1.03	0.83	0.14	0.21	16.2	7.5	3.69	126	94
20–40	28	29.2	12.9	0.11	0.99	0.81	0.16	0.23	13.7	6.4	3.94	131	105
40–60	10	30.9	11.8	0.10	0.94	0.82	0.18	0.27	12.7	5.7	3.60	120	113
60–80	1	29.5	8.5	0.08	0.96	1.05	0.19	0.21	16.1	6.7	3.38	n.d.	n.d.
>80	0												

weight against Mn:Fe ratios of nodules at each station (Figure 11) is not particularly useful because the principal variation between stations is one of nodule size rather than Mn:Fe ratio. Taken together with the data from areas *C* and *F*, this suggests that this graphical plot of Craig (1979) serves no useful purpose.

The most important factor controlling the differences in composition between nodules from different stations and locations at area *G* results from the dilution of the ferromanganese oxide material in the nodules by volcanic rock fragments in the nodule (see section on morphology). Judging by the reduction of Mn content of the nodules, this is equivalent to the incorporation of perhaps 30% and more by weight of volcanic rock fragments in some of the nodules. This effect is particularly marked in comparing nodules from Locs 16–18 characterized by higher Mn:Fe ratios; higher Ni, Cu, and Zn contents; and lower Fe contents (Co remains about the same) with those from Locs 20, 21, and 23 immediately south of the main fault zone where incorporation of volcanic rock fragments into the nodules is more pronounced. The fact that the 40–60 mm size fraction of the nodules has higher Mn, Cu, and Zn and lower Fe contents than the smaller nodules suggests that these larger nodules have, on average, incorporated marginally lesser amounts of these fragments in the nodules. These volcanic rock fragments often have a reddish color due to iron staining and this accounts for the enhancement of the Fe contents of the nodules containing these fragments. These chemical data therefore show quite categorically that the composition of area *G* nodules is related not only of diagenetic processes related to the dissolution of siliceous organisms on the seafloor but also to the "seeding" of the nodule and the relative extent of incorporation of iron-rich volcanic rock fragments. This latter process is much more marked in the region south of the main fault zone. The influence of geological processes in the morphology and composition of nodules in this area is therefore emphasized.

Interestingly, Craig (1979) states that "survey area VA-4, adjacent to a group of seamounts, shows a definite bulk compositional trend toward higher Fe content and lower Mn:Fe ratios compared to areas without large volcanic features" and suggests a volcanic influence for these "hydrothermal type" deposits. However, the nodule compositions reported at VA-4 are more likely the result of
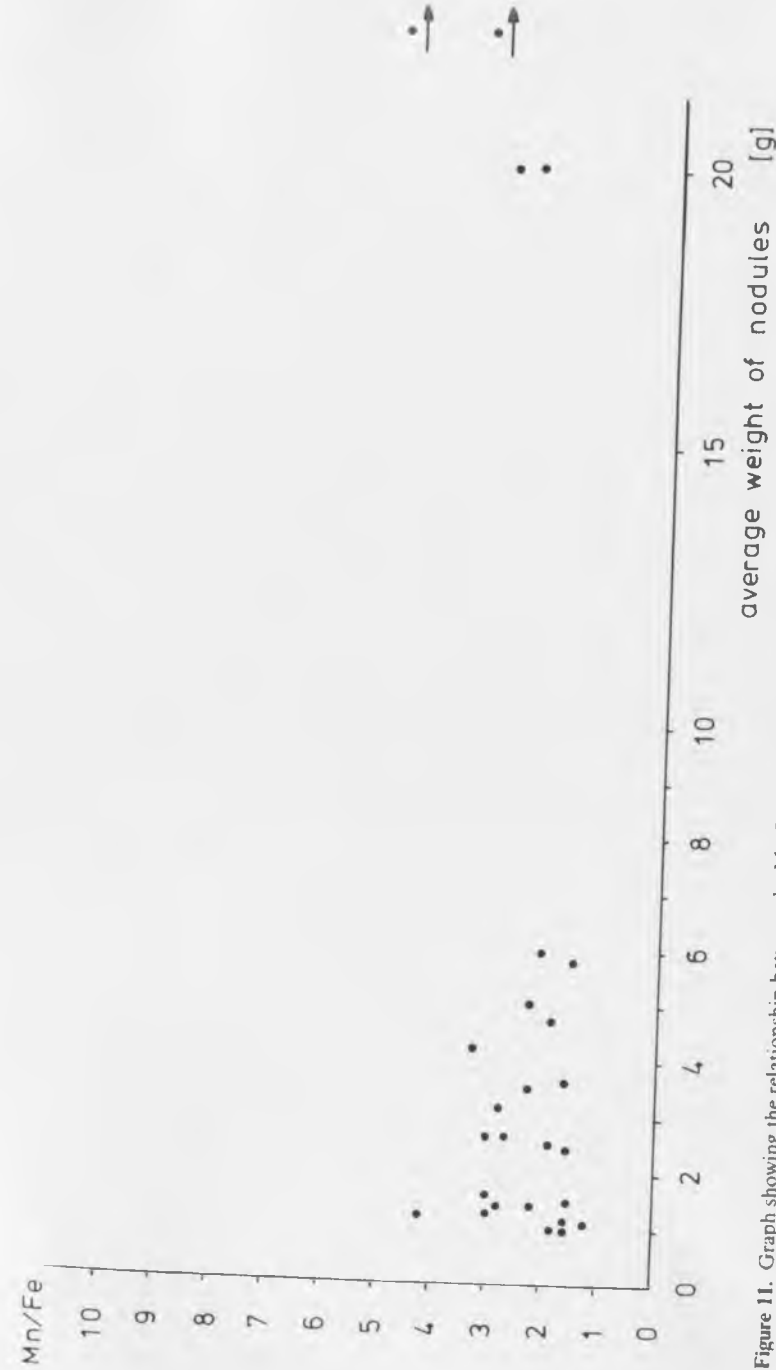

Figure 11. Graph showing the relationship between the Mn:Fe ratio and the average weight of nodules from each station at area *G* following the method of Craig (1979).

the incorporation of volcanic fragments in the nodules (as in area *G*) than the factors suggested by Craig for which there is no direct geological evidence.

Mineralogy

X-ray diffraction analysis of six nodules and one crust showed todorokite and δ-MnO$_2$ to be the principal manganese oxide phases with quartz and feldspar and/or zeolite to be the silicate minerals (Table 17). In the manganese crust from Stn 137 GK, zeolite is more abundant than the manganese minerals. This higher silicate content may account in part for the low transition metal contents of these crusts. There appears to be no difference in the mineralogy of nodules from north and south of the Marquesas Fracture Zone.

Discussion

The preceding sections have described in some detail the principal characteristics of manganese nodules from three areas (*C*, *F*, and *G*) in the equatorial Pacific and established differences both within these areas and regionally. In this section, it is relevant to try to elucidate some of the factors controlling the observed regional differences in nodule characteristics.

It is here proposed that the main features of the nodules can best be explained in terms of the influence of the biological productivity of the overlying surface waters on nodule characteristics as previously proposed by a number of authors (e.g., Greenslate, 1974a,b; Dugolinsky, 1976; Arrhenius et al., 1979; Leclaire and Perseil, 1979; Margolis et al., 1979; Callender and Bowser, 1980; Frazer and Fisk, 1981). In this hypothesis, siliceous organisms in areas of high biological productivity such as the equatorial high-productivity belt in the Pacific (cf. Berger, 1970, Figure 4) are assumed to sink to the seafloor, decompose and liberate certain trace metals (notably Ni, Cu, and Mn) into the pore waters; these elements can then ultimately be incorporated into the overlying manganese nodules, particularly on the underside, thus causing their enrichment in the nodules. Nodules from such areas are therefore characterized by high concentrations of these elements relative to normal pelagic

Table 17

X-ray diffraction analysis of nodules and crust from area *G*. The principal mineral phases present are underlined.

Stn	Size Fraction (mm)	Definite	Probable
99 GB	0–20	Todorokite, δ-MnO$_2$	Feldspar
114 KG	20–40	Todorokite, δ-MnO$_2$	Quartz, Feldspar and/or Zeolite
119 GB	0–20	Todorokite, δ-MnO$_2$	Quartz, Feldspar and/or Zeolite
120 GB	0–20	Todorokite, δ-MnO$_2$	Feldspar
133 GB	0–20	Todorokite, δ-MnO$_2$	Quartz, Feldspar and/or Zeolite
137 GK	Crust-type C	Zeolite, Todorokite, δ-MnO$_2$	
145 GB	0–20	Todorokite, δ-MnO$_2$	Feldspar and/or Zeolite

nodules from red clay environments in regions of low biological productivity such as beneath the temperate-latitude oceanic gyres. Heath (1974) has excellently reviewed the silica cycle in the ocean (cf. Hurd, 1973; Johnson, 1974, 1976; Schink et al., 1975; Schink and Guinasso, 1977; von Rad 1979; Hein et al., 1979a; Barron and Whitman, 1981; Kastner, 1981) and the dissolution of siliceous tests on the seafloor. In addition, Halbach et al. (1979) and Marchig et al. (1979) have shown that dissolution of manganese micronodules in the sediment column may play a role in remobilizing these transition elements in pelagic sediments and Callender and Bowser (1980) have suggested that Mn may be deposited in pelagic sediments predominantly with terrigenous particles. With the possible exception of Mn, however, these transition elements are ultimately derived from dissolution of siliceous tests.

From the brief area descriptions given in the Introduction, it can be seen that area *C* is a zone of high biological productivity characterized by the presence of siliceous ooze and of low sedimentation

rates due to the erosional influence of bottom waters. The high biological productivity favors the formation of nodules characterized by high Mn:Fe ratios (average 5.4) and Ni + Cu contents (average 2.48%). The low sedimentation rate favors the growth of large nodules (average nodule weight 92.6 g) and moderately high nodule abundance (average 4.9 kg/m²). The fact that the strong erosional surface can be traced back to the Lower Miocene (Van Andel et al., 1975, Fig. 25) has led to an interesting development. Because of the long time scale involved, an older generation of nodules has grown, which has fragmented in situ to form the nuclei on which the larger (>60 mm) nodules have subsequently grown; Heye (1975) has described the methods by which such fragmentation can occur. The smaller (<40 mm) nodules found in area C represent a discrete, younger population of nodules. The extremely low sedimentation rates at area C would favor nodule formation not only because of slow burial rates of the nodules but also because of the highly oxidized nature of the sediments. Bramlette (1961) (quoted in Arrhenius, 1963) has stated that "the redox state of the sediment is mainly determined by the duration of contact with the oxidizing bottom water."

Area D is a region of high (calcareous) sedimentation rate just north of the equator where nodules are absent.

Area F is an area of high productivity (characterized by the presence of siliceous debris) and moderately high calcareous sedimentation (Van Andel et al., 1975, Figure 38). Here, the nodules are characterized by high Mn:Fe ratios (average 4.8) and the highest Ni + Cu contents encountered (average 2.54%) but, because of the high sedimentation rates, the nodules are small (average nodule weight 2.4 g) and nodule abundance is low (average 1.3 kg/m²).

Area G to the south of area F is more towards the margin of the belt of high productivity. It is therefore characterized by a lower carbonate-free opal content of the sediment (Van Andel et al. 1975, Figure 5) than area F. The nodules are characterized by lower Mn:Fe ratios (average 2.2) and lower Ni + Cu contents (average 1.81%) but, because of the lower sedimentation rates, nodules are somewhat larger (average nodule weight 2.5 g) and nodule abundance higher (average 3.1 kg/m²) than at area F. This somewhat simple picture is complicated at area G by the complex morphology

of the nodules, which results from the incorporation of angular volcanic fragments into many of the nodules, particularly in the region immediately south of the main fault zone. While this process has clearly significantly influenced the bulk composition of the nodules in area G (see above), the biogenic factor remains the major influence on the composition of the ferromanganese oxide phase of nodules in this area. Neither area F nor G is characterized by the erosive conditions encountered at area C (Van Andel et al., 1975, Figure 25). Only young immature nodules are therefore present in these two areas and the larger, mature (second generation) nodules found at area C are absent.

Further south of these areas is the low productivity, subtropical anticyclonic gyre beneath which lie the Southwestern Pacific and Samoan Basins (Glasby et al., 1980). Here, nodules reach a density in excess of 20 kg/m², have Mn:Fe ratios of the order of unity and Ni + Cu contents of the order of 0.4 – 0.6% and lie on red clay. These nodules may be considered to be true pelagic nodules which are formed dominantly by the direct deposition of elements from seawater with no influence of the effects of high biological activity as in the equatorial Pacific.

Pautot and Melguen (1979) have suggested that the greatest abundance of nodules is encountered in a 300–400-m thick layer situated between the lysocline and the carbonate compensation depth (C.C.D.). Whilst this relationship may appear to hold for areas F and G from a comparison of data in Table 18 with those in Figure 7, it does not hold for area C (or for area K in the Aitutaki Passage) which lies exclusively below the C.C.D. It is felt to be an artifact for areas F and G because these areas lie entirely above the C.C.D. and therefore sampling beneath the C.C.D. is impossible. The lower average abundance of nodules at areas F and G compared with area C is related to the higher carbonate contents of these sediments. Although low carbonate contents (and therefore depths below the lysocline and preferably the C.C.D.) are essential for high nodule abundance because of the requirement for nodule growth of low sedimentation rates, the data do not support Pautot and Melguen's assertion that highest nodule abundances are found above the C.C.D. Skornyakova (1979), for example, states clearly that the highest nodule abundances are confined to depths below

Table 18
Position of the lysocline and C.C.D. at areas *C*, *F*, and *G*.

Area	Lysocline	C.C.D.
C	-	< 4,650
F	4,400	5,000
G	4,200–4,300	4,900–5,000

Data from Melguen (Friedrich et al. 1979, pp. 149–206). Depths in meters.

the C.C.D.

Considering the above N–S equatorial transect, the central role of biological productivity on nodule size, abundance, grade (and therefore economic potential) can readily be seen. The influence of diagenetic effects due to the decomposition of siliceous organisms within the sediment column is most marked at area *F* where the Ni and Cu contents of the nodules are highest but the nodule density is low because of the effects of high carbonate sedimentation. The presence of carbonate material in area *F* sediments may indeed increase the rate of diagenesis of the siliceous ooze (Kastner et al., 1977) and therefore increase the Ni and Cu contents of the nodules. At area *G*, on the margins of the high-productivity belt, the diagenetic effects are somewhat reduced (lower Ni + Cu contents) but the nodule density is higher because the carbonate sedimentation rate is lower. Beneath the subtropical anticyclonic gyre (in regions well removed from land such that terrigenous sedimentation rates are low), diagenetic effects due to the dissolution of siliceous microfossils are absent and the nodules are characterized by lower Ni + Cu contents (the Ni + Cu here being derived principally from direct depositions from seawater). However, the low sedimentation rates (due to the absence of biogenic sedimentation) permit extremely high nodule abundances. Only at area *C*, characterized by bottom current erosion since the Lower Miocene, are the effects of diagenetic enrichment of Ni + Cu in the nodules compatible with high nodule abundance resulting from low sedimentation rates. The correlation between high nodule abundance and low sedimentation rate can be seen by inspection of the sediment isopach data of Ludwig and Houtz (1979) which show clearly that abundant nodule deposits generally form when the total sediment thickness is less than 100 m. Data from area *C* therefore emphasize the importance of oceanic bottom currents as well as

biological productivity of the overlying surface waters in controlling nodule characteristics. Of course, the precise mode of formation of nodules at area *C* presented here is not incompatible with those presented by von Stackelberg (1979) for equatorial North Pacific nodules and many of the ideas expressed here are an extension of those first put forward by Greenslate et al. (1973). In particular, these latter authors show a relationship between nodule and sediment composition in the equatorial Pacific which is quite compatible with the above arguments. The data presented here would also support Menard and Frazer's (1978) contention that nodule grade and abundance are negatively correlated (cf. Moritani, 1979; Frazer and Fisk, 1981) (although only under certain circumstances) in contrast to the assumption of Archer (1976) that these two parameters are independent. The data would also suggest that nodules from the equatorial S. Pacific (at least in the vicinity of areas *F* and *G*) do not have any major economic potential (cf. Frazer, 1977).

Comparison of the composition of nodules from the Aitutaki Passage (area *K*), a region of low biological productivity beneath the subtropical anticyclonic gyre, with those from the equatorial Pacific (Table 19) including the data for Mo, Pb, and Ti (Table 20), and Tl (Table 21) (cf. Glasby et al., 1978), reveals a marked difference in composition for all elements. In particular, Mn, Ni, Cu, Zn, Ba, Mo, and Tl are present in higher concentrations and Fe, Co, SiO_2, Al_2O_3, U, La, Ce, Pb, and Ti in lower concentrations in equatorial Pacific nodules. Rankin and Glasby (1979) also found a number of other elements lower in the equatorial Pacific compared to Southwest Pacific nodules. Of the elements analyzed, therefore, only Mn, Ni, Cu, Zn, Ba, Mo, and Tl are enriched in the equatorial Pacific nodules and this would suggest that these are the only elements enriched in nodules as a result of the diagenetic effects of the decomposition of biological organisms on the seafloor. It should be noted, however, that barite occurs in the acid-insoluble residue of the nodule as shown by X-ray diffraction. The other elements (e.g., Fe, Co, U, La, Ce, Pb, and Ti) would appear not to be involved in such processes but rather be derived principally by the direct deposition from seawater. The lower content of these elements in equatorial Pacific nodules may in fact merely reflect the dilution of these elements in nodules characterized by higher deposition rates of Mn,

Table 19
Average composition of nodules from areas C, F, G, and K. All analyses in percent, except where otherwise stated.

Area	Location Nos.	No. of Analyses	Mn	Fe	Co	Ni	Cu	Zn	Ba	SiO_2	Al_2O_3	U ppm	Ce ppm	La ppm
C	1–6	40	29.1	5.4	0.23	1.29	1.19	0.16	0.33	16.1	6.0	3.32	259	105
F	8–15	107	32.0	6.7	0.11	1.23	1.31	0.18	0.23	15.2	5.0	3.08	110	90
G	16–23	90	28.4	12.8	0.12	1.00	0.81	0.15	0.22	15.4	7.0	3.76	125	100
Average		237	29.8	8.3	0.15	1.18	1.13	0.16	0.26	15.6	6.0	3.39	165	98
K (Aitutaki Passage)	24–37	161	14.9	17.3	0.42	0.36	0.16	0.06	0.14	19.8	8.4	7.76	n.a.*	172

*Not analyzed.

Table 20
Analytical data for Ti, Mo, and Pb in selected nodules from different stations in areas C, F, and G.

Area	Loc	Stn	Size Fraction (mm)	Ti (%)	Mo (ppm)	Pb (ppm)
C	1	2 GB	30–40	0.22	860	280
			20–30	0.23	890	380
			0–20	0.19	840	320
	2	8 GB	60–80	0.42	920	410
			40–60	0.29	780	360
			20–40	0.29	970	360
			0–20	0.31	780	360
	4	19 GB	>100	0.30	780	360
			80–100	0.29	890	400
			60–80	0.36	980	380
			20–40	0.22	920	300
			Average	0.28	874	355
F	10	53 GB 59 GB	20–40	0.18	740	140
			60–80	0.16	530	120
			40–60	0.25	600	220
			20–40	0.18	630	170
			10–20	0.16	690	130
			0–10	0.19	510	130
	11	63 GB	60–80	0.19	430	100
			40–60	0.19	460	120
	11	63 GB	60–80 Outer zone	0.21	460	120
			Core	0.16	410	85
	12	74 KAL	broken nodule	0.21	470	130
	14	85 GB	20–40	0.20	510	150
			10–15	0.19	600	150
			5–10	0.22	340	170
	15	89 GB	80–100	0.24	370	130
			15–20	0.19	460	190
			5–15	0.21	380	170
			0–5	0.22	150	120
	15	95 GR	20–40	0.19	380	130
			15–20	0.20	480	150
			10–15	0.22	400	150
			0–10	0.21	250	130
			Average	0.19	472	140

G. Friedrich, G. P. Glasby, T. Thijssen, W. L. Plüger

G	16	99 GB	40-60	0.34	570	150
			20-30	0.32	570	150
			15-20	0.34	510	150
			10-15	0.31	510	170
			5-10	0.34	420	130
			0-5	0.36	310	170
			broken nodule	0.31	540	150
	17	114 KG	40-60	0.51	280	130
			20-40	0.39	410	180
			10-20	0.38	380	
		119 GB	20-40	0.35	560	130
			15-20	0.34	530	130
			10-15	0.35	460	120
			0-10	0.37	460	130
	20	131 GB	15-20	0.50	460	200
			0-10	0.56	340	200
	21	137 DK	60-80	0.44	480	100
			40-60	0.35	370	130
			30-40	0.32	510	100
		137 DK*	A crust 0-5mm	1.70	130	660
			A crust 5-10mm	1.43	220	560
			B crust	1.26	250	360
			D crust	0.68	240	350
	23	147 GB	20-30	0.46	400	230
			10-20	0.44	350	230
			0-10	0.54	220	220
			bulk sample	0.59	130	170
			Average	0.40	425	157

*These values not included in the average.

Table 21

Analytical data for Tl in selected nodules from different stations in areas C, F, and G. Analyses in ppm.

Area	Loc	Stn	Size Fraction (mm)	Tl
C	1	2 GB	20-30	66
	2	8 GB	20-40	150
			60-80	173
	4	19 GB	>100	146
			Average	129
F	10	53 GB	20-40	119
		59 GB	60-80	170
	12	74 KAL	broken nodule	133
	14	89 GB	5-15	87
			Average	127
G	16	99 GB	15-20	133
	20	131 GB	15-20	144
	21	137 DK	60-80	230
		137 DK*	A crust 5-10 mm	113
	23	147 GB	10-20	114
			Average	155

*This value not included in the average.

Ni, Cu, and Zn; this is a result of the requirement that the manganese oxide phase, iron oxide phase, and silicate phase must add to 100% (Glasby, 1973). The higher silicate content of the Aitutaki Passage nodule may also merely act as a diluent for the authigenic elements, although the higher contents of Fe and Ti in these nodules may be partially attributed to incorporation in the silicate minerals (cf. Ruppert, 1979). Fe and Ti are also higher in sediments from the Aitutaki Passage compared with those of the equatorial Pacific; this has been attributed to the higher proportion of basaltic material in the sediments there (Stoffers et al., 1981). The difference in silicate composition of equatorial Pacific and Aitutaki Passage nodules (Table 19) is, however, not large enough to account for differences in the Tl content of nodules by dilution with the silicate phase as suggested by Glasby et al. (1978). A similar association of elements to that noted above has been reported by a number of authors (e.g., Ostwald and Frazer, 1973; Calvert and Price, 1977; Lyle et al., 1977; Moorby and Cronan, 1981; Piper and Williamson,

1981; Roy, 1981; Li, 1982). The ubiquity of this pattern of element association suggests that the relationship between the biological productivity of the overlying surface water and nodule mineralogy and element enrichment patterns may be fundamental to an understanding of nodule genesis.

From the above, it is possible to compute the approximate enrichment sequence of elements in nodules as a result of this diagenetic process. Comparing area F which has the maximum Cu:Ni ratio (Mn, 32.0%; Ni, 1.23%; Cu, 1.31%; Zn, 0.18%; Ba, 0.23%; Mo, 472 ppm; Tl, 127 ppm) and the Aitutaki Passage (Mn, 14.9%; Ni, 0.36%; Cu, 0.16%; Zn, 0.06%; Ba, 0.14%; Mo, 216 ppm; Tl, 76 ppm) (Tables 19 – 21), it is seen that the element-enrichment sequence in nodules from the belt of equatorial high productivity compared with those from a normal red clay environment is Cu 8.2 > Ni 3.4 > Zn 3.0 > Mo 2.2 ≈ Mn 2.1 > Tl 1.7 ≈ Ba 1.6.

Although these figures are only intended as an illustration, they do indicate that Cu is the element most enriched in nodules as a result of enhanced biological activity (cf. Arrhenius et al., 1979) and are in accord with the findings of Calvert and Price (1977), who showed by factor analysis an element-correlation pattern Mn - Ni - Cu - Zn - Ba - Mo - Mg in nodules. These ideas are also supported by the work of Marchig et al. (1979) on the diagenesis of radiolarian oozes (cf. Marchig and Gundlach, 1979; 1981; 1982). The data also indicate that the Cu:Ni ratios of the nodules are not constant but vary from 0.44 for Aitutaki Passage nodules (area K) to 1.06 for area F nodules where they reach a maximum. These data therefore show that the association of Ni and Cu in nodules is not as close as is commonly assumed.

On the basis of a detailed chemical study of the composition of plankton, sediment, and nodules from the equatorial North Pacific using selective leaching techniques, Boylan et al. (1980) have shown that the major part of the Ni and Cu in the equatorial North Pacific nodules had its origin in planktonic organisms (cf. Colley et al., 1979; Boyle, 1981). The decreasing Cu:Ni ratio in the sequence plankton–sediment–nodule (Boylan et al., 1980, Table 2) would support the idea that more Cu than Ni is available in planktonic organisms for the enrichment in nodules from the higher productiv-

ity belt. The flux of Cu across the sediment–water interface has been computed by Boyle et al. (1977), Klinkhammer (1980), and Callender and Bowser (1980). It should be noted, however, that in Peru Basin nodules (Thijssen et al., 1981), Ni (1.14%) exceeds Cu (0.62%) to give a Cu:Ni ratio of 0.54. The Cu enrichment is therefore not always as pronounced as in the equatorial Pacific belt (cf. Halbach et al., 1981). The data also show that Zn is also derived partially from such diagenetic processes in equatorial Pacific nodules and this helps to explain the well-known Mn - Ni - Cu - Zn correlation in manganese nodules (cf. Cronan, 1975). Finally, Arrhenius et al. (1979) have presented some interesting ideas on how these elements are taken up into the manganese oxide structure and, in particular, in the way in which molybdate ion substitutes for the manganate ion in crystal lattice. A good theoretical explanation for the observed element associations is therefore becoming available.

An interesting observation also comes from the analysis of manganese crusts from areas F (Stn 94) and G (Stn 137) (see Appendix) which shows that the crusts contain significantly lower contents of Mn, Ni, Cu, and Mo and higher contents of Fe, SiO$_2$, Al$_2$O$_3$, Ti, and Pb from the same areas. The data for Stn 137 crusts confirm the conclusion of Lyle et al. (1977) that the normal authigenic precipitation of ferromanganese oxides from seawater controls the composition of manganese crusts while nodule composition is governed by small-scale diagenetic reactions in the sediment. However, X-ray diffraction analysis of a manganese crust from Stn 137 shows that zeolite is the principal mineral present and that the principal manganese oxide minerals are todorokite and δ-MnO$_2$ as for the area G nodules (Table 17). For the crust from Stn 94, the much higher silicate content of the crust is the major factor in lowering the contents of Mn, Ni, Cu, and Zn in the crusts, although the lowered diagenetic contribution is also probably important. Differences in the origins of the crusts and nodules are therefore emphasized.

The above data are also generally compatible with the conclusions of Piper and Williamson (1977) regarding the occurrence of high Mn/Fe and Ni + Cu nodules in the Pacific (see also Calvert and Price, 1977; Calvert et al., 1978). These authors' conclusions must, however, now be modified in light of the newly established

relations between biological productivity, sedimentation rate, and nodule composition and abundance at the southern margins of the belt of equatorial high productivity in the Pacific; this is a situation that is fundamentally different in terms of sedimentation rate but not biological productivity from that encountered in the equatorial North Pacific on which much of Piper and Williamson's evidence for the origin of high Mn/Fe and Ni + Cu nodules is based. The above conclusions on the relationship between nodule composition, abundance, sedimentation rate, and biological productivity are also supported by Japanese work in the Central Pacific Basin where nodules with higher abundance and lower Mn/Fe and Ni + Cu contents are found on deep-sea clay, whereas nodules with lower abundance and higher Mn/Fe and Ni + Cu contents are found on siliceous clays (see Mizuno and Moritani, 1977, p. 145 [Figure XIV-4], p. 166 [Table XVI-3]). The above data also suggest that the distribution map for copper for Pacific nodules produced by Skornyakova and Andrushchenko (1974, p. 914 [Figure 125]) needs revising in view of the findings here of nodules from south of the equator containing >1% Cu.

An interesting corollary of the above discussion stems from the work of Boudreau and Scott (1978, also cf. Elderfield, 1976). These authors have suggested, on the basis of mathematical models, that the growth of manganese nodules is dependent mainly on the diffusion-controlled flux of manganese and other trace elements through the benthic boundary layer from seawater rather than from the underlying pore water. Although this conclusion is undoubtedly true for nodules formed in red-clay environments, it is not strictly valid for nodules from the equatorial belt of high productivity. Here, trace metals (notably Ni, Cu, and Mn) are released for incorporation into the micronodules and macronodules by the in situ decomposition of siliceous frustules within the sediment. The factor controlling the release of these metals into pore water is therefore the decomposition of these frustules within the sediment column and not the redox characteristics of the metals per se. The stability field of the siliceous frustules is therefore the most important factor in the diagenetic migration of Ni, Cu, and Mn in this type of environment. In addition, Hein et al. (1979a,b) have concluded that authigenic smectite in equatorial Pacific sediments results from the

reaction of dissolving biogenic debris with iron hydroxide; this may be an additional factor in fixing iron in the sediment rather than in the nodule phase. This type of diagenesis is therefore quite different in character from that encountered in shallow-water, continental margin environments such as described by Ku and Glasby (1972). The data do, however, conform with the conclusion of Heye and Marchig (1977) that faster growth rates of nodules result in higher concentration of Ni, Cu, and Mn, which is a logical extension of the ideas presented above.

Finally, Usui (1979) has suggested that the uptake of transition metals into manganese nodules is controlled by the mineralogy and suggested that the atomic ratio of the incorporated metals relative to manganese into 10 Å manganite is about 0.17 (1/6). In the nodules studied here, the atomic ratio (Cu + Ni + Co + Zn)/Mn is generally less than 0.10. However, these represent bulk and not microprobe analyses and no data are available for the Ca and Mg contents of the manganese oxide phase. 10 Å manganite forms the principal manganese oxide phase of the equatorial Pacific nodule compared with δ-MnO$_2$ for Aitutaki Passage nodules. The role of divalent metal ions (particularly of Ni, Cu, and Zn ions) in stabilizing 10 Å manganite seems, therefore, to be established (Giovanoli et al., 1975; Giovanoli and Brütsch, 1979). Glasby and Thijssen (1982) have suggested that it is the supply of these divalent metal ions from the sediment column during diagenesis that controls the formation of Å manganite as well as nodule composition. More careful attention should therefore be paid to the role of sediment diagenesis in controlling nodule mineralogy and geochemistry. The previously observed relationship between nodule mineralogy and composition (e.g., Calvert and Price, 1977) would appear to be controlled by such diagenetic processes. Burns and Burns (1978a,b) have also suggested a relationship between biological productivity and mineralogy. The way is therefore open for a comprehensive theory of nodule formation linking biological productivity to nodule mineralogy and geochemistry.

This study has therefore evaluated in a more quantitative manner than before the role of biological productivity at both the northern and southern margins of the belt of equatorial high productivity in controlling nodule genesis. It is clear from this work that more

detailed latitudinal transects are required to evaluate the precise role of biological, hydrological, and sedimentological processes in controlling nodule type at these margins. This should become a central problem in manganese nodule research.

Acknowledgments

References

Archer, A. A., 1976, Prospects for the exploitation of manganese nodules: the main technical, economic and legal problems. *CCOP/SOPAC Technical Bulletin*, Vol. 2, pp. 21–38.

Arrhenius, G., 1952, Sediment cores from the East Pacific. *Reports of the Swedish Deep-Sea Expedition.*, Vol. V.

Arrhenius, G., 1963, Pelagic sediments. In: *The Sea*, Hill, M. N., ed., Wiley-Interscience, New York, Vol. 3, pp. 655–727.

Arrhenius, G., Cheung, K., Crane, S., Fisk, M., Frazer, J., Korkisch, J., Mellin, T., Nakkao, S., Tsai, A., and Wolf, G., 1979, Counterions in marine manganates. *Colloques Internationaux du C.N.R.S.*, No. 289, pp. 333–356.

Bäcker, H., Glasby, G. P., and Meylan, M. A., 1976, Manganese nodules from the Southwestern Pacific Basin. *NZOI Oceanographic Field Report*, No. 6: 88 pp.

Barron, E. J., Whitman, J. M., 1981, Oceanic sediments in space and time. In: *The Sea*, Emiliani, C., ed., Wiley-Interscience, New York, Vol. 7, pp. 689–731.

Berger, W. H., 1970, Biogenous deep-sea sediments: fractionation by deep-sea circulation. *Bulletin of the Geological Society of America*, Vol. 81, pp. 1385–1402.

Berger, W. H., Adelseck, C. G., and Mayer, L. A., 1976, Distribution of carbonate in surface sediments of the Pacific Ocean. *Journal of Geophysical Research*, Vol. 81, pp. 2617–2627.

Bischoff, J. L., and Piper, D. Z. (eds.), 1979, *Marine Geology and Oceanography of the Pacific Manganese Nodule Province*. Plenum Press, New York, 842 pp.

Boudreau, B. R., and Scott, M. R., 1978, A model for the diffusion-controlled growth of deep-sea manganese nodules. *American Journal of Science*, Vol. 278, pp. 903–929.

Boylan, D. B., Rutgers, S., Zeitlin, H., and Andrews, J. E., 1980, A comparative study of copper, nickel, and cobalt trace metal species in plankton, sediment, and manganese nodules from the equatorial North Pacific. *Marine Mining*, Vol. 2, pp. 171–189.

Boyle, E. A., 1981, Cadmium, zinc, copper, and barium in foraminifera tests. *Earth and Planetary Science Letters*, 53: 11–35.

Boyle, E. A., Sclater, F. R., and Edmond, J. M., 1977, The distribution of dissolved copper in the Pacific. *Earth and Planetary Science Letters*, Vol. 37, pp. 38–54.

Bramlette, M. N., 1961, Pelagic sediments. In: *Oceanography*. American Association for the Advancement of Science Publication, Vol. 67, pp. 345–366.

Burns, V. M., and Burns, R. G., 1978a, Post-depositional metal enrichment processes inside manganese nodules from the north equatorial Pacific. *Earth and Planetary Science Letters*, Vol. 39, pp. 341–348.

Burns, V. M., and Burns, R. G., 1978b, Authigenic todorokite and phillipsite inside deep-sea manganese nodules. *American Mineralogist*, Vol. 63, pp. 827–831.

Callender, E., and Bowser, C. J., 1980, Manganese and copper geochemistry of interstitial fluids from manganese nodule-rich pelagic sediments of the northeastern equatorial Pacific Ocean. *American Journal of Science*, Vol. 280, pp. 1063–1096.

Calvert, S. E., and Price, N. B., 1977, Geochemical variation in ferromanganese nodules and associated sediments from the Pacific Ocean. *Marine Chemistry*, Vol. 5, pp. 43–74.

Calvert, S. E., and Price, N. B., Heath, G. R., Moore, T. C., 1978, Relationship between ferromanganese nodule composition in a small survey area of the equatorial Pacific. *Journal of Marine Research*, Vol. 36: 161–183.

Colley, N. M., Cronan, D. S., and Moorby, S. A., 1979, Some geochemical and mineralogical studies on newly collected ferromanganese oxide deposits from the North West Indian Ocean. *Colloques Internationaux du C.N.R.S.*, No. 289, pp. 13–21.

Craig, J. D., 1979, The relationship between bathymetry and ferromanganese deposits in the north equatorial Pacific. *Marine Geology*, Vol. 29, pp. 165–186.

Craig, J. D., and Andrews, J. E., 1978, A factor analysis study of deep-sea ferromanganese deposits in the equatorial North Pacific Ocean. *Marine Mining*, Vol. 1, pp. 305–326.

Cronan, D. S., 1975, Zinc in marine manganese nodules. *Transactions of the Institution of Mining and Metallurgy*, Vol. 84B, pp. 30–32.

Dudley, W. C., 1979, Biogenic influence on the composition and structure of marine manganese nodules. *Colloques Internationaux du C.N.R.S.*, No. 289, pp. 227–232.

Dugolinsky, B. K., 1976, Chemistry and morphology of deep-sea manganese nodules and the significance of associated encrusting protozoans on nodule growth. Ph.D. thesis, University of Hawaii, 229 pp.

Edmond, J. M., Chung, Y. and Sclater, J. G., 1971, Pacific bottom water: penetration east around Hawaii. *Journal of Geophysical Research*, Vol. 76, pp. 8089–8097.

Elderfield, H., 1976, Manganese fluxes to the oceans. *Marine Chemistry*, Vol. 4, pp. 103–132.

Felix, D., 1980, Some problems in making nodule abundance estimates from sea floor photographs. *Marine Mining*, Vol. 2, pp. 293–302.

Frazer, J. Z., 1977, Manganese nodule reserves: an updated estimate. *Marine Mining*, Vol. 1, pp. 103–123.

Frazer, J. Z., and Fisk, M. B., 1981, Geological factors related to characteristics of sea-floor manganese nodule deposits. *Deep-Sea Research*, Vol. 28A, pp. 1533–1551.

Friedrich, G., 1979, Fahrtbericht und wissenschaftlicher Zwischenbericht der Fahrten So 06/1 und /2 mit F.S. *Sonne* "Hawaii-Tahiti-Transect" Teilprojekt ICIME August-Oktober 1978. Technische Hochschule Aachen. 288 pp. (Unpublished Report).

Friedrich, G., Glasby, G. P., Plüger, W. L., and Thijssen, T., 1981, Results of the recent exploration for manganese nodules in the South Pacific by R. V. Sonne. *Inter Ocean (Dusseldorf)*, IO 81-302/01, pp. 72–81.

Giovanoli, R., and Brütsch, R., 1979, Über oxidhydroxide des Mn (IV) unit Schichtengitter. 5. Mitteilung, Austauschverhalten und die Rolle bei Bildung von Tiefsee-Mangankonkretionen. *Chimia*, Vol. 33, pp. 372–376.

Giovanoli, R., Bürki, P., Giuffredi, M., and Stumm, W., 1975, Layer structured manganese oxide hydroxides. IV: The buserite group; structure stabilization by transition elements. *Chimia*, Vol. 29, pp. 517–520.

Glasby, G. P., 1973, Manganese deposits of variable composition from north of the Indian-Antarctic Ridge. *Nature Physical Science*, Vol. 242, pp. 106–108.

Glasby, G. P., 1977, Why manganese nodules remain at the sediment-water interface. *N. Z. Journal of Science*, Vol. 20, pp. 187–190.

Glasby, G. P., Keays, R. R., and Rankin, P. C., 1978, The distribution of rare earth, precious metal and other trace elements in Recent and fossil deep-sea manganese nodules. *Geochemical Journal*, Vol. 12, pp. 229–243.

Glasby, G. P., Meylan, M. A., Margolis, S. V., and Backer, H., 1980, Manganese deposits of the Southwestern Pacific Basin. In: *Geology and Geochemistry of Manganese*, Varentsov, I. M., and Grasselly, Gy., eds., Hungarian Academy of Sciences, Budapest, Vol. 3, pp. 137–183.

Glasby, G. P., and Thijssen, T., 1982. Control of the mineralogy and composition of marine manganese nodules by the supply of divalent transition metal ions *Neues Jahrbuch für Mineralogie*.

Greenslate, J., 1974a, Micro-organisms participate in the construction of manganese nodules. *Nature*, [Lond.], Vol. 249, pp. 181–183.

Greenslate, J., 1974b, Manganese and biotic debris associations in some deep-water sediments. *Science*, Vol. 186, pp. 529–531.

Greenslate, J. L., Frazer, J. Z., and Arrhenius, G., 1973, Origin and deposition of selected transition elements in the seabed. In: *Papers on the Origin and Distribution of Manganese Nodules in the Pacific and Prospects for Exploration*, Morgenstein, M., ed., Hawaii Institute of Geophysics, pp. 45–70.

Halbach, P., and Ozkara, M., 1979, Morphological and geochemical classification of deep-sea ferromanganese nodules and its genetical interpretation. *Colloques Internationaux du C.N.R.S.*, No. 289, pp. 77–88.

Halbach, P., Rehm, E., and Marchig, V., 1979, Distribution of Si, Mn, Fe, Ni, Cu, Co, Zn, Pb, Mg, and Ca in grain-size fractions of sediment samples from a manganese nodule field in the Central Pacific Ocean. *Marine Geology*, Vol. 29, pp. 237–252.

Halbach, P., Sherhag, C., Hebisch, U., and Marchig, V., 1981, Geochemical and mineralogical control of different genetic types of deep-sea nodules from the Pacific Ocean. *Mineralium Deposita*, Vol. 16, pp. 59–84.

Heath, G. R., 1974, Dissolved silica and deep-sea sediments. *Society of Economic Paleontologists and Mineralogists Special Publication*, Vol. 20, pp. 77–93.

Heath, G. R., 1979, Burial rates, growth rates, and size distributions of deep-sea manganese nodules. *Science*, Vol. 205, pp. 903–904.

Hein, J. R., Ross, C. R., Alexander, E., and Yeh, H.-W., 1979a, Mineralogy and diagenesis of surface sediments from DOMES, A, B, and C. In: *Marine Geology and Oceanography of the Pacific Managanese Nodule Province*, Bischoff, J. L., and Piper, D. Z., eds., Plenum Press, New York, pp. 365–396.

Hein, J. R., Yeh, H.-W., and Alexander, E., 1979b, Origin of iron-rich montmorillonite from the manganese nodule belt of the north equatorial Pacific. *Clays and Clay Minerals*, Vol. 27, pp. 185–194.

Heye, D., 1975, Wachstumsverhältnisse von Manganknollen. *Geologisches Jahrbuch*, Vol. 5E, pp. 3–122.

Heye, D., 1979, Relationship between the size of manganese nodules in the Central Pacific, their chemical constitution and other parameters. *Colloques Internationaux du C.N.R.S.*, No. 289, pp. 89–91.

Heye, D., and Marchig, V., 1977, Relationship between the growth rate of manganese nodules from the Central Pacific and their chemical constitution. *Marine Geology*, Vol. 23, pp. M19–M25.

Hurd, D. C., 1973, Interactions of biogenic opal, sediment and seawater in the Central Equatorial Pacific. *Geochimica et Cosmochimica Acta*, Vol. 37, pp. 2257–2282.

Johnson, T. C., 1974, The dissolution of siliceous microfossils in surface sediments of the eastern tropical Pacific. *Deep-Sea Research*, Vol. 21, pp. 851–864.

Johnson, T. C., 1976, Biogenic opal preservation in pelagic sediments of a small area in the eastern tropical Pacific. *Bulletin of the American Geological Society*, Vol. 87, pp. 1273–1282.

Karas, M. C., and Greenslate, J., 1979, Marine manganese concretions: shape and size related growth models. *Deep-Sea Research*, Vol. 26A, pp. 809–824.

Kastner, M., 1981, Authigenic silicates in deep-sea sediments: Formation and diagenesis. In: *The Sea*, Emiliani, C., ed., Wiley-Interscience, New York, Vol. 7, pp. 915–980.

Kastner, M., Keene, J. B., and Gieskes, J. M., 1977, Diagenesis of siliceous oozes. I. Chemical controls in the rate of opal-A to opal-CT transformation - an experimental study. *Geochimica et Cosmochimica Acta*, Vol. 41, pp. 1041–1059.

Klinkhammer, G. P., 1980, Early diagenesis in sediments from the eastern equatorial Pacific. II. Pore water metal results. *Earth and Planetary Science Letters*, Vol. 49, pp. 81–101.

Ku, T. L., and Glasby, G. P., 1972, Radiometric evidence of rapid growth rates of shallow-water, continental margin manganese nodules. *Geochimica et Cosmochimica Acta*, Vol. 36, pp. 699–703.

Leclaire, L., and Perseil, E.-A., 1979, Minéralogie, composition chimique et milieux de sédimentation de concrétions polymétalliques dans l'Ocean Indien. *Colloques Internationaux du C.N.R.S.*, No. 289, pp. 23–37.

Li, Y.-H., 1982, Interelement relationship in abyssal Pacific ferromanganese nodules and associated pelagic sediments. *Geochimica et Cosmochimica Acta*.

Ludwig, W. J., and Houtz, R. E., 1979, Isopach map of sediments in the Pacific Ocean Basin and marginal sea basins. Chart published by American Association of Petroleum Geologists.

Lyle, M., Dymond, J., and Heath, G. R., 1977, Copper-nickel enriched ferromanganese nodules and associated crusts from the Bauer Basin, northwest Nazca Plate. *Earth and Planetary Science Letters*, Vol. 35, pp. 55–64.

Mallik, T. K., 1980, Macro- and micromorphology of some manganese nodules from the Indian Ocean. *Marine Geology*, Vol. 34, pp. M45–M56.

Marchig, V., and Gundlach, H., 1979, Changes in chemical composition of some Pacific manganese nodules during their growth. In: *Marine Geology and Oceanograpny of the Pacific Manganese Nodule Province*, Bischoff, J. L., and Piper, D. Z., eds., Plenum Press, New York, pp. 729–746.

Marchig, V., and Gundlach, H., 1981, Separation of iron from manganese and growth of manganese nodules as a consequence of diagenetic ageing of radiolarians,. *Marine Geology*, Vol. 40, pp. M34–M43.

Marchig, V., and Gundlach, H., 1982, Material balance in manganese nodule formation (North Central Pacific). *Geochimica et Cosmochimica Acta*, Vol. 46, pp. 693–695.

Marchig, V., Gundlach, H., and Schnier, C., 1979, Verhalten von Radiolarienschalen aus dem Zentralpazifik bei der Diagenese. *Geologische Rundschau*, Vol. 68, pp. 1037–1054.

Margolis, S. V., Dugolinsky, B. K., and Dudley, W. C., 1979, Microchemistry and morphology of biogenic detrital and authigenic phases in Pacific manganese nodules. *Colloques Internationaux du C.N.R.S.*, No. 289, pp. 179–209.

Menard, H. W., and Frazer, J. Z., 1978, Manganese nodules on the sea floor: inverse correlation between grade and abundance. *Science*, [N.Y.], Vol. 199, pp. 969–971.

Meyer, K., 1973, Surface sediment and manganese nodule facies, encountered on R/V Valdivia cruises 1972/73. In: *Papers on the Origin and Distribution of Manganese Nodules in the Pacific and Prospects for Exploration*, Morgenstein, M., ed., Hawaii Institute of Geophysics, pp. 125–130.

Meylan, M. A., Glasby, G. P., McDougall, J. C., and Singleton, R. J., 1978, Manganese nodules and associated sediments from the Samoan Basin and Passage. *NZOI Oceanographic Field Report*, No. 11, 61 pp.

Mizuno, A., ed., 1981, Deep sea mineral resources investigation in the northern part of the Central Pacific Basin January–March 1979 (GH79-1 Cruise). *Geological Survey of Japan Cruise Report*, No. 15, 309 pp.

Mizuno, A., and Moritani, T., eds., 1977, Deep sea mineral resources investigation in the central-eastern part of the Central Pacific Basin January–March 1976 (GH 76-1 Cruise). *Geological Survey of Japan Cruise Report*, No. 8, 217 pp.

Mizuno, A., Miyazaki, T., and Nishimura, A., 1980, Central Pacific manganese nodules, and their relation to sedimentary history. *Proceedings of the Offshore Technology Conference OTC*, 3830, pp. 331–336.

Moorby, S. A., and Cronan, D. S., 1981, The distribution of elements between coexisting phases in some marine ferromanganese oxide deposits. *Geochimica et Cosmochimica Acta*, Vol. 45, pp. 1855–1877.

Moore, W. S., Ku, T.-L., Macdougall, J. D., Burns, V. M., Burns, R., Dymond, J., Lyle, M. W., and Piper, D. Z., 1981, Fluxes of metals to a manganese nodule: radiochemical, chemical, structural and mineralogical studies. *Earth and Planetary Science Letters*, Vol. 52, pp. 151–171.

Moritani, T., ed., 1979, Deep sea mineral resources investigations in the central-western part of the Central Pacific Basin January–March 1977 (GH 77-1 Cruise). *Geological Survey of Japan Cruise Report*, No. 12, 256 pp.

Moritani, T., Maruyama, S., Nohara, M., Kinoshita, Y., Ogitsu, T., and Moriwaki, H., 1977, Description, classification, and distribution of manganese nodules. *Geological Survey of Japan Cruise Report*, No. 8, pp. 136–158.

Moritani, T., and Nakao, S., eds., 1981, Deep sea mineral resources investigation in the western part of Central Pacific Basin January–March 1978 (GH 78-1 Cruise). *Geological Survey of Japan Cruise Report*, No. 17, 281 pp.

Ostwald, J., and Frazer, F. W., 1973, Chemical and mineralogical investigations on deep sea manganese nodules from the Southern Ocean. *Mineralium Deposita*, Vol. 8, pp. 303–311.

Paul, A. Z., 1976, Deep-sea bottom photographs show that benthic organisms remove sediment cover from manganese nodules. *Nature*, [Lon.], Vol. 263, pp. 50–51.

Pautot, G., and Melguen, M., 1979, Influence of deep water circulation and sea floor morphology on the abundance and grade of central South Pacific man-

ganese nodules. In: *Marine Geology and Oceanography of the Pacific Manganese Nodule Province*, Bischoff, J. L., and Piper, D. Z., eds., Plenum Press, New York, pp. 621;nd649.

Piper, D. Z., Leong, K., and Cannon, W. F., 1979a, Manganese nodule and surface sediment compositions: DOMES sites A, B, and C. In: *Marine Geology and Oceanography of the Pacific Manganese Nodule Province*, Bischoff, J. L., and Piper, D. Z., eds., Plenum Press, New York, pp. 437;473.

Piper, D. Z., Cook, H. E., and Gardener, J. V., 1979b, Lithic and acoustic stratigraphy of the equatorial North Pacific: DOMES sites A, B, and C. In: *Marine Geology and Oceanography of the Pacific Manganese Nodule Province*, Bischoff, J. L., and Piper, D. Z., eds., Plenum Press, N.Y., pp. 309–348.

Piper, D. Z., and Williamson, M. E., 1977, Composition of Pacific Ocean ferromanganese nodules. *Marine Geology*, Vol. 23, pp. 285–303.

Piper, D. Z., and Williamson, M. E., 1981, Mineralogy and composition of concentric layers within a manganese nodule from the North Pacific Ocean. *Marine Geology*, Vol. 40, pp. 255–268.

Raab, W., 1972, Physical and chemical features of Pacific deep sea manganese nodules and their implications to the genesis of nodules. In: *Ferromanganese Deposits of the Ocean Floor*, Horn, D. R., ed., National Science Foundation, Washington, D.C., pp. 31–49.

Raab, W. J., and Meylan, M. A., 1977, Morphology. In: *Marine Manganese Deposits*, Glasby, G. P., ed., Elsevier, Amsterdam, pp. 109–146.

Rankin, P. C., and Glasby, G. P., 1979, Regional distribution of rare earth and inor elements in manganese nodules and associated sediments in the Southwest Pacific and other localities. In: *Marine Geology and Oceanography of the Pacific Manganese Nodule Province*, Bischoff, J. L., and Piper, D. Z., eds., Plenum Press, New York, pp. 681–697.

Roy, S., 1981, *Manganese Deposits*. Academic Press. Inc., London. 458 pp.

Ruppert, H., 1979, Microstratigraphic chemical investigations of Mn-Fe nodules from the northern equatorial Pacific. *Chemie der Erde*, Vol. 38, pp. 265–291.

Schink, D. R., and Guinasso, N. L., 1977, Effects of bioturbation in sediment-seawater interaction. *Marine Geology*, Vol. 23, pp. 133–154.

Schink, D. R., Guinasso, N. L., and Fanning, K. A., 1975, Processes affecting the concentration of silica at the sediment-water interface of the Atlantic Ocean. *Journal of Geophysical Research*, Vol. 80, pp. 3013–3031.

Skornyakova, N. S., 1979, Zonal regularities in occurrence, morphology and chemistry of manganese nodules of the Pacific Ocean. In: *Marine Geology and Oceanography of the Pacific Manganese Nodule Province*, Bischoff, J. L., and Piper, D. Z., eds., Plenum Press, New York, pp. 699–727.

Skornyakova, N. S., and Andrushchenko, P. F., 1974, Iron-manganese concretions in the Pacific Ocean. *International Geology Review*, Vol. 16, pp. 863–919.

Sorem, R. K., and Banning, D. L., 1976. Microfeatures of typical manganese nodules from six box cores from NOAA cruise RP6-OC-75. In: *Deep Ocean Mining Environmental Study, NE Pacific Nodule Province, Site, C, Geology and*

Geochemistry. Bischoff, J. L., and others, eds., U.S. Geological Survey Open-File Report, Vol. 76–548, 275 pp.

Sorem, R. K., and Fewkes, R. H., 1980, Distribution of todorokite and birnessite in manganese nodules from the "Horn region," eastern Pacific Ocean. In: *Geology and Geochemistry of Manganese*, Vol. 1, Varentsov, I. M., and Grasselly, Gy, eds., Hungarian Academy of Sciences, Budapest, pp. 203–463.

Sorem, R. K., Fewkes, R. H., McFarland, W. D., Reinhart, W. R., 1979, Physical aspects of the growth of manganese nodules in the "Horn Region," east equatorial Pacific Ocean. *Colloques Internationaux du C.N.R.S.*, No. 289, pp. 61–76.

Stoffers, P., Glasby, G. P., Thijssen, T., Shrivastava, P. C., and Melguen, M., 1981, The geochemistry of coexisting manganese nodules, micronodules, sediments and pore waters from five areas in the equatorial and S. W. Pacific. *Chemie der Erde*, Vol. 40, pp. 273–297.

Thijssen, T., Glasby, G. P., Schmitz-Wiechowski, A., Friedrich, G., Kunzendorf, H., Muller, D., and Richter, H., 1981, Reconnaissance survey of manganese nodules from the northern sector of the Peru Basin. *Marine Mining*, Vol. 2, pp. 285–428.

Uchio, T., 1976, Studies of deep-sea manganese nodules (Part I). *Journal of the Faculty of Engineering, the University of Tokyo (B)*, Vol. 33, pp. 611–625.

Usui, A., 1979, Mineralogical study of marine manganese nodule, synthesis of hydrous manganese oxides, and their implications to genesis and geochemistry. Ph.D. thesis, University of Tokyo, 175 pp.

Van Andel, Tj. H., Heath, G. R., and Moore, T. C., 1975, Cenozoic history and paleoceanography of the central equatorial Pacific Ocean. *Memoir of the Geological Survey of America*, Vol. 143, 134 pp.

Von Rad, U., 1979, SiO$_2$ - Diagenese in Tiefseesedimenten. *Geologische Rundschau*, Vol. 68, pp. 1025–1036.

Von Stackelberg, U., 1979, Sedimentation, hiatuses and development of manganese nodules (Valdivia Site VA-13/2, northern central Pacific). In: *Marine Geology and Oceanography of the Pacific Manganese Nodule Province*, Bischoff, J. L., and Piper, D. Z., eds., Plenum Press, New York, pp. 559–586.

Appendix

Analytical data of manganese nodules from different stations in areas C, F, and G, central North Pacific, R. V. *Sonne* cruise SO-06/1, 1978. All analyses in percent, except where otherwise stated. For convenience, the following abbreviations are used: GB, Free Fall Grab; DK, Dredge; KG, Spade Corer; KAL Box Corer.

Table A1
Analytical data of manganese nodules from area G.

Location	Station No.	Size mm	Mn	Fe	Co	Ni	Cu	Zn	Ba	SiO$_2$	Al$_2$O$_3$	U ppm	Ce ppm	La ppm
17	114 KG	40 - 60	24.7	13.5	0.10	0.96	0.68	0.13	0.18	18.3	8.3	3.65	150	150
		20 - 40	31.6	12.7	0.12	1.13	0.96	0.16	0.21	10.9	6.0	4.09	115	90
		10 - 20	29.8	12.2	0.13	1.22	0.89	0.15	0.17	13.0	7.0	4.00	110	100
		∅	29.4	12.8	0.12	1.11	0.87	0.15	0.19	14.1	7.1	3.91	125	113
17	Average (114)		29.4	12.8	0.12	1.11	0.87	0.15	0.19	14.1	7.1	3.91	125	113
18	115 GB	20 - 40	25.7	16.7	0.16	0.82	0.57	0.12	0.21	11.6	5.7	5.21	220	120
		15 - 20	25.5	16.9	0.15	0.82	0.58	0.12	0.20	12.5	6.9	4.39	175	130
		∅	25.6	16.8	0.16	0.82	0.58	0.12	0.21	12.6	6.3	4.80	198	125
	116 GB	20 - 40	23.8	15.8	0.16	0.77	0.51	0.11	0.17	15.8	7.2	4.87	210	140
		10 - 20	24.3	16.4	0.16	0.81	0.53	0.11	0.17	15.5	7.5	4.72	190	120
		< 10	28.2	16.4	0.16	0.93	0.70	0.13	0.16	11.6	5.8	5.07	200	110
		∅	25.4	16.2	0.16	0.84	0.58	0.12	0.17	14.3	6.8	4.89	200	123
	118 GB	20 - 40	31.0	11.9	0.12	2.23	0.89	0.16	0.24	10.9	6.3	3.80	80	90
		10 - 20	30.4	12.3	0.12	1.15	0.90	0.16	0.29	11.6	6.1	3.58	115	90
		< 10	26.3	13.5	0.13	1.10	0.83	0.13	0.20	17.9	7.7	3.18	90	90
		∅	29.2	12.6	0.12	1.12	0.87	9.15	0.24	13.5	6.7	3.52	95	90
	119 GB	20 - 40	32.4	9.5	0.09	1.09	1.02	0.20	0.19	11.9	6.0	4.02	55	n.d.
		15 - 20	31.6	9.4	0.10	1.14	1.06	0.19	0.17	12.9	6.3	3.98	60	n.d.
		10 - 15	30.2	9.5	0.10	1.15	1.07	0.18	0.21	14.7	7.1	3.62	50	n.d.
		< 10	29.3	10.0	0.11	1.26	1.10	0.15	0.17	15.9	7.6	3.17	70	n.d.
		∅	31.2	9.6	0.10	1.14	1.05	0.18	0.19	13.9	6.8	3.70	59	n.d.

Table A1 (cont.)

Location	Station No.	Size mm	Mn	Fe	Co	Ni	Cu	Zn	Ba	SiO$_2$	Al$_2$O$_3$	U ppm	Ce ppm	La ppm
	120 GB	20 - 40	32.8	11.6	0.11	1.03	0.93	0.19	0.33	10.3	5.4	4.08	130	130
		10 - 20	32.5	11.9	0.11	1.12	0.98	0.18	0.34	10.0	5.6	4.06	170	100
		< 10	32.3	12.4	0.12	1.15	0.93	0.18	0.36	10.0	5.6	4.12	180	120
		∅	32.5	12.0	0.11	1.10	0.95	0.18	0.34	10.1	5.5	4.09	160	117
	121 GB	20 - 40	26.4	15.3	0.13	0.99	0.68	0.14	0.31	14.2	6.8	4.35	180	180
		10 - 20	28.8	15.0	0.13	1.05	0.76	0.15	0.29	12.8	6.7	4.18	160	160
		< 10	27.9	13.4	0.14	1.14	0.85	0.14	0.24	15.1	7.7	3.74	140	90
		∅	27.7	14.6	0.13	1.06	0.76	0.14	0.28	14.0	7.1	4.09	160	143
	122 GB	20 - 40	28.5	12.7	0.12	1.15	0.83	0.15	0.25	15.1	7.0	3.83	160	100
		10 - 20	26.6	12.2	0.11	1.13	0.77	0.15	0.25	17.9	7.7	3.62	130	100
		< 10	28.9	12.7	0.13	1.19	0.90	0.15	0.21	14.2	7.2	3.77	100	100
		∅	28.0	12.5	0.12	1.16	0.83	0.15	0.24	15.7	7.3	3.74	130	100
	123 KG	40 - 60	22.0	17.9	0.14	0.75	0.48	0.10	0.20	16.6	7.5	4.80	220	290
		20 - 40	19.4	18.4	0.13	0.59	0.44	0.10	0.16	19.1	7.7	4.68	210	180
		10 - 20	24.8	17.7	0.15	0.81	0.57	0.12	0.21	13.7	6.5	5.08	230	140
		∅	22.1	18.0	0.14	0.72	0.50	0.11	0.19	16.5	7.2	4.85	220	203
	124 KG	40 - 60	32.7	10.2	0.09	1.10	1.00	0.19	0.25	10.9	5.4	3.91	130	80
		brok.nod. 20 - 40	31.9	10.8	0.10	1.07	0.97	0.20	0.24	11.4	5.6	3.96	100	100
		brok.nod. < 20	32.4	11.0	0.10	0.99	0.94	0.20	0.25	10.9	5.6	3.82	90	90
		∅	32.2	10.7	0.10	1.05	0.97	0.20	0.25	11.1	5.5	3.90	107	90

G. Friedrich, G. P. Glasby, T. Thijssen, W. L. Plüger

Table A1 (cont.)

Location	Station No.	Size mm	Mn	Fe	Co	Ni	Cu	Zn	Ba	SiO$_2$	Al$_2$O$_3$	U ppm	Ce ppm	La ppm
18	Average (115-124)		28.2	13.7	0.13	1.01	0.79	0.15	0.23	13.5	6.6	4.18	148	116
20	127 GB	20 - 40	22.9	15.0	0.11	0.90	0.64	0.12	0.20	21.2	8.6	3.53	130	130
		10 - 20	20.7	10.7	0.09	0.87	0.63	0.11	0.18	26.8	10.7	2.74	110	90
		< 10	17.5	12.1	0.09	0.76	0.58	0.09	0.16	30.6	11.6	2.11	100	85
		∅	20.4	12.6	0.10	0.84	0.62	0.11	0.18	26.2	10.3	2.79	113	102
	128 GB	20 - 40	22.2	14.0	0.12	0.80	0.57	0.10	0.18	24.0	9.9	3.79	140	110
		10 - 20	23.5	13.9	0.12	0.89	0.64	0.11	0.20	22.6	9.6	3.57	160	120
		< 10	17.4	13.3	0.10	0.68	0.49	0.09	0.16	30.1	11.1	2.55	130	90
		∅	21.0	13.7	0.11	0.79	0.57	0.10	0.18	25.6	10.2	3.30	143	107
	130 GB	20 - 30	25.1	15.6	0.13	0.86	0.66	0.13	0.23	16.3	7.2	4.22	180	140
		∅	25.1	15.6	0.13	0.86	0.66	0.13	0.23	16.3	7.2	4.22	180	140
	131 GB	15 - 20	26.9	14.0	0.13	1.05	0.77	0.14	0.22	16.1	7.6	4.23	170	130
		< 10	26.0	13.5	0.12	1.06	0.79	0.13	0.16	18.5	8.5	3.72	90	90
		∅	26.5	13.8	0.13	1.06	0.78	0.14	0.19	17.3	8.1	3.98	130	110
	132 GB	20 - 40	27.5	13.1	0.12	1.08	0.85	0.14	0.24	16.6	7.7	3.84	140	100
		10 - 20	24.8	13.3	0.12	0.98	0.75	0.14	0.17	19.0	8.2	3.83	130	100
		< 10	19.0	13.1	0.09	0.83	0.66	0.09	0.15	27.6	10.4	−	130	90
		∅	23.8	13.2	0.11	0.96	0.75	0.12	0.18	21.1	8.8	3.84	133	97
	133 GB	20 - 40	28.2	12.2	0.11	1.01	0.93	0.17	0.18	14.6	6.5	4.01	70	n.d.
		15 - 20	31.6	8.3	0.08	1.13	1.14	0.20	0.16	14.4	6.9	3.82	70	n.d.
		10 - 15	29.8	8.7	0.09	1.20	1.12	0.18	0.16	17.0	7.7	3.72	90	n.d.

Table A1 (cont.)

Location	Station No.	Size mm	Mn	Fe	Co	Ni	Cu	Zn	Ba	SiO$_2$	Al$_2$O$_3$	U ppm	Ce ppm	La ppm
		< 10	25.9	9.4	0.09	1.13	1.00	0.14	0.15	22.6	9.1	2.94	60	n.d.
		∅	28.9	9.7	0.09	1.12	1.04	0.17	0.16	17.2	7.6	3.62	73	n.d.
	138 KG	40 - 60	30.8	12.5	0.11	0.83	0.78	0.16	0.36	14.5	4.5	3.21	70	n.d.
		∅	30.8	12.5	0.11	0.83	0.78	0.16	0.36	14.5	4.5	3.21	70	n.d.
20	Average (127-138)		25.2	13.0	0.11	0.92	0.74	0.13	0.21	19.7	8.1	3.57	120	94
21	137 DK	60 - 80	29.5	8.5	0.08	0.96	1.05	0.19	0.21	16.1	6.7	3.38	n.d.	n.d.
		40 - 60	27.9	13.0	0.09	0.86	0.73	0.17	0.24	15.5	6.2	3.09	100	90
		20 - 40	29.3	7.9	0.07	0.93	1.01	0.21	0.24	15.8	7.7	3.95	100	80
		30 - 40	31.2	11.3	0.09	1.01	0.91	0.18	0.38	12.9	5.4	3.46	100	80
		20 - 30	29.8	14.1	0.13	1.08	0.83	0.17	0.25	11.8	5.9	4.40	140	100
		20 - 20	32.5	12.2	0.13	1.13	0.83	0.19	0.29	10.0	5.8	3.98	150	110
		15 - 20	29.4	13.0	0.12	1.12	0.87	0.17	0.28	12.5	5.7	3.98	160	80
		10 - 15	30.0	12.6	0.12	1.13	0.87	0.17	0.22	13.7	7.0	3.83	100	80
		< 10	27.8	14.3	0.13	1.12	0.87	0.14	0.18	16.1	8.1	3.58	100	80
		∅	29.7	13.1	0.11	1.03	0.88	0.18	0.25	13.8	6.5	3.73	111	83
21	Average (137)		29.7	13.1	0.11	1.03	0.88	0.18	0.	13.8	6.5	3.73	111	83
21	137 DK*	crust A outer zone												
		0 - 5	20.6	20.7	0.38	0.36	0.06	0.09	0.15	12.0	4.5	7.69	500	150
		10 - 5	17.9	21.4	0.36	0.19	0.05	0.07	0.19	16.4	7.1	7.05	500	200
		crust B	22.1	20.2	0.17	0.51	0.36	0.11	0.22	15.0	5.4	6.02	300	150
		crust D	21.8	0.18	0.30	0.19	0.08	0.20		21.9	7.0	5.27	280	170

Morphology and Geochemistry of Manganese Nodules

Table A2 (cont.)
Analytical data of manganese nodules from area *C*.

Location	Station No.	Size mm	Mn	Fe	Co	Ni	Cu	Zn	Ba	SiO$_2$	Al$_2$O$_3$	U ppm	Ce ppm	La ppm
	10 KG	20 - 40	27.3	6.0	0.27	1.41	1.23	0.13	0.30	21.8	7.7	3.00	240	110
		brok. nod.	23.9	5.7	0.23	1.34	1.01	0.12	0.31	19.7	7.5	3.17	250	100
		ø	25.6	5.9	0.25	1.38	1.12	0.13	0.31	20.8	7.6	3.09	245	105
2	Average (7-10)		26.9	5.8	0.25	1.32	1.12	0.15	0.29	18.0	6.7	3.27	243	108
3	23 GB	60 - 80	30.0	4.8	0.23	1.25	1.13	0.15	0.44	15.0	4.8	3.82	265	120
		30 - 40	31.4	4.8	0.29	1.40	1.62	0.15	0.38	17.1	6.3	2.93	225	90
		20 - 30	32.9	4.4	0.25	1.42	1.43	0.16	0.37	16.5	6.1	3.07	205	100
		ø	31.4	4.7	0.26	1.36	1.39	0.15	0.40	16.2	5.7	3.27	232	103
	24 GB	80 -100	28.4	6.1	0.20	1.21	0.99	0.16	0.34	14.7	5.9	3.55	330	130
		0 - 20	29.9	5.8	0.21	1.40	1.20	0.15	0.38	16.5	6.1	3.28	295	100
		ø	29.2	6.0	0.21	1.31	1.10	0.16	0.36	15.6	6.0	3.42	313	115
	25 GB	>100	31.3	5.4	0.21	1.12	1.00	0.15	0.33	15.5	5.9	3.31	310	100
		ø	31.1	5.4	0.21	1.12	1.00	0.15	0.33	15.5	5.9	3.31	310	100
	25 GB*	>100 outer zone	31.2	7.1	0.23	1.21	0.89	0.16	0.24	13.9	5.4	3.89	340	120
		middle zone	28.1	5.2	0.18	1.16	1.04	0.15	0.36	16.0	6.1	3.28	300	120
		core	36.5	3.4	0.26	0.94	1.08	0.15	0.64	11.3	4.6	2.30	260	110
	26 KAL	80 -100	28.8	5.7	0.19	1.28	1.05	0.16	0.38	13.9	5.7	3.35	260	110
		ø	28.8	5.7	0.19	1.28	1.05	0.16	0.38	13.9	5.7	3.35	260	110

Table A2 (cont.)
Analytical data of manganese nodules from area *C*.

Location	Station No.	Size mm	Mn	Fe	Co	Ni	Cu	Zn	Ba	SiO$_2$	Al$_2$O$_3$	U ppm	Ce ppm	La ppm
3	Average (23-26)		30.1	5.5	0.22	1.27	1.14	0.16	0.37	15.3	5.8	3.34	279	107
4	13 GB	60 - 80	28.0	5.8	0.20	1.26	1.08	0.16	0.33	15.0	6.0	3.27	280	110
		20 - 40	28.9	3.4	0.19	1.44	1.49	0.14	0.25	13.4	5.3	5.17	175	120
		ø	28.5	4.6	0.20	1.35	1.29	0.15	0.29	14.2	5.7	4.22	228	115
	14 GB	brok. nod.	31.5	6.3	0.24	1.03	0.94	0.15	0.37	13.9	5.4	3.61	330	120
		ø	31.5	6.3	0.24	1.03	0.94	0.15	0.37	13.9	5.4	3.61	330	120
	15 GB	80 -100	28.4	6.3	0.23	1.15	0.99	0.14	0.37	14.7	5.8	3.58	325	110
		ø	28.4	6.3	0.23	1.15	0.99	0.14	0.37	14.7	5.8	3.58	325	110
	16 GB	>100	32.2	5.7	0.24	1.12	1.01	0.18	0.31	13.1	4.9	3.52	315	80
		ø	32.2	5.7	0.24	1.12	1.01	0.18	0.31	13.1	4.9	3.52	315	80
	18 GB	>100	28.0	6.5	0.22	1.14	0.94	0.15	0.27	15.0	5.7	3.54	315	110
		60 - 80	29.6	6.4	0.22	1.19	1.07	0.14	0.36	14.4	5.5	3.65	325	120
		ø	28.8	6.5	0.22	1.17	1.01	0.15	0.32	14.7	5.6	3.60	325	120
	19 GB	> 100	26.5	6.4	0.22	1.11	0.93	0.16	0.34	15.0	5.3	3.45	320	110
		80 -100	30.0	6.1	0.26	1.16	1.05	0.15	0.36	15.5	5.6	3.34	265	90
		60 - 80	30.9	5.2	0.23	1.31	1.13	0.16	0.39	15.5	5.6	3.35	260	90
		40 - 60	30.3	5.5	0.24	1.43	1.11	0.16	0.33	15.0	5.7	3.75	285	100
		20 - 40	32.1	4.2	0.21	1.43	1.38	0.17	0.35	16.5	6.0	3.12	200	100
		ø	30.0	5.5	0.23	1.29	1.12	0.16	0.35	15.5	5.6	3.40	266	98
	20 GB	80 -100	21.3	6.0	0.24	1.27	1.10	0.15	0.40	15.5	6.0	3.46	265	130

Table A2 (cont.)

Analytical data of manganese nodules from area C.

Location	Station No.	Size mm	Mn	Fe	Co	Ni	Cu	Zn	Ba	SiO$_2$	Al$_2$O$_3$	U ppm	Ce ppm	La ppm
		20 - 40	34.8	3.6	0.19	1.51	1.48	0.18	0.31	16.0	5.8	3.04	180	80
			28.1	4.8	0.22	1.39	1.29	0.17	0.36	15.8	5.9	3.25	223	105
	21 GB	80 -100	28.7	6.8	0.20	1.17	0.90	0.16	0.26	14.4	5.7	3.62	305	110
		20 - 40	34.3	3.9	0.18	1.49	1.47	0.18	0.34	15.5	5.8	3.21	160	90
		∅	31.5	5.4	0.19	1.33	1.19	0.17	0.30	15.0	5.8	3.42	233	100
	21 GB*	80 -100	31.2	7.0	0.22	1.28	0.96	0.16	0.23	13.9	4.5	3.85	350	120
		outer zone	29.8	5.4	0.17	1.16	0.97	0.15	0.36	13.9	6.0	3.44	315	120
		middle zone	34.2	4.7	0.26	0.98	0.99	0.11	0.74	12.3	4.8	2.72	235	100
	22 GB	core	28.5	6.3	0.22	1.22	1.00	0.16	0.33	15.5	5.8	3.33	310	90
		> 100	29.9	5.7	0.20	1.37	1.11	0.16	0.36	15.0	5.7	3.45	285	120
		80 - 100												
		∅	29.2	6.0	0.21	1.30	1.06	0.16	0.35	15.3	5.8	3.39	298	105
	22 GB*	> 100	32.7	6.4	0.20	1.26	0.94	0.19	0.22	13.4	5.1	3.67	300	110
		outer zone	28.7	6.8	0.20	1.15	0.88	0.16	0.28	15.0	5.8	3.75	290	110
		middle zone	33.6	4.6	0.26	1.06	1.09	0.12	0.66	13.9	5.3	2.40	250	120
		core												
4	Average (13 - 22)		29.8	5.7	0.22	1.23	1.10	0.16	0.30	14.7	5.6	3.55	283	106

*These samples not included in average values.

Table A3

Analytical data of manganese nodules from area F.

Location	Station No.	Size mm	Mn	Fe	Co	Ni	Cu	Zn	Ba	SiO$_2$	Al$_2$O$_3$	U ppm	Ce ppm	La ppm
8	37 GB	20 - 40	31.8	7.1	0.11	1.30	1.35	0.17	0.20	14.4	4.7	–	100	90
		15 - 20	32.1	7.1	0.12	1.29	1.37	0.17	0.20	14.6	4.6	3.27	100	85
		8 - 10	30.9	7.4	0.13	1.40	1.37	0.16	0.20	16.0	5.3	2.89	115	80
		5 - 8	29.3	8.5	0.13	1.31	1.29	0.16	0.18	17.6	5.3	–	95	100
		3 - 5	27.5	9.1	0.14	1.35	1.30	0.14	0.19	21.2	5.7	–	110	80
		∅	30.7	7.7	0.13	1.33	1.35	0.16	0.19	16.3	5.0	3.11	103	88
8	Average (37)		30.7	7.7	0.13	1.33	1.35	0.16	0.19	16.3	5.0	3.11	103	88
9	49 GB	20 - 40 + 15 - 20	35.3	4.6	0.08	1.25	1.47	0.22	0.28	11.8	4.3	3.68	105	80
		∅	35.3	4.6	0.08	1.25	1.47	0.22	0.28	11.8	4.3	3.68	105	80
	50 GB	15 - 20	35.6	4.7	0.08	1.18	1.46	0.22	0.24	12.3	4.5	–	100	90
		∅	35.6	4.7	0.08	1.18	1.46	0.22	0.24	12.3	4.5	–	100	90
9	Average (49-50)		35.5	4.7	0.08	1.22	1.47	0.22	0.26	12.1	4.4	3.68	103	85
10	52 GB	60 - 80	33.7	6.6	0.10	1.06	1.03	0.20	0.39	11.3	3.8	2.46	100	90
		40 - 60	35.3	6.8	0.12	1.36	1.40	0.17	0.26	12.1	4.0	3.32	110	80
		20 - 40	35.1	6.3	0.12	1.38	1.46	0.18	0.21	12.4	4.5	3.38	100	90
		15 - 20	33.5	6.8	0.12	1.41	1.44	0.17	0.21	14.4	5.3	3.38	100	90
		10 - 15	34.0	6.6	0.13	1.41	1.47	0.17	0.20	14.7	4.8	3.09	110	80
		< 10	31.0	7.6	0.13	1.30	1.47	0.15	0.22	17.1	5.3	3.11	95	100
		∅	33.8	6.8	0.12	1.32	1.38	0.17	0.25	13.7	4.6	2.80	100	80
													3.03	103	87

Table A3 (cont.)

Analytical data of manganese nodules from area *F*.

Location	Station No.	Size mm	Mn	Fe	Co	Ni	Cu	Zn	Ba	SiO₂	Al₂O₃	U ppm	Ce ppm	La ppm
	53 GB	20 - 40	35.4	5.7	0.11	1.38	1.47	0.19	0.23	12.6	4.4	3.40	100	90
		∅	35.4	5.7	0.11	1.38	1.47	0.19	0.23	12.6	4.4	3.40	100	90
	54 GB	20 - 40	31.3	8.1	0.13	1.24	1.22	0.16	0.27	13.8	4.4	3.07	125	85
		15 - 20	29.7	8.3	0.13	1.25	1.23	0.14	0.18	19.7	6.2	–	120	90
		brok.nod.	30.2	11.5	0.20	1.04	0.96	0.13	0.23	11.6	4.3	4.50	200	130
		∅	30.4	9.3	0.15	1.18	1.14	0.14	0.23	15.0	5.0	3.79	148	102
	55 GB	20 - 40	34.6	5.1	0.09	1.24	1.43	0.21	0.25	11.3	4.0	3.57	110	80
		15 - 20	35.7	4.5	0.09	1.25	1.49	0.22	0.26	12.6	4.3	3.52	105	90
		10 - 15	34.8	5.0	0.09	1.29	1.52	0.20	0.25	15.0	4.8	3.38	100	80
		∅	35.0	4.9	0.09	1.26	1.48	0.21	0.25	13.0	4.4	3.49	105	83
	57 GB	15 - 20	34.8	4.7	0.09	1.27	1.52	0.21	0.28	12.3	4.0	3.44	105	80
		∅	34.8	4.7	0.09	1.27	1.52	0.21	0.28	12.3	4.0	3.44	105	80
	59 GB	60 - 80	33.9	5.9	0.09	1.05	1.18	0.18	0.48	12.5	3.4	2.59	80	80
		40 - 60	33.0	6.7	0.12	1.14	1.35	0.16	0.40	12.5	3.9	3.10	120	80
		20 - 40	33.7	5.9	0.10	1.28	1.44	0.18	0.23	12.5	4.2	3.36	100	90
		10 - 20	34.1	5.2	0.09	1.26	1.48	0.20	0.23	13.2	4.6	3.42	115	70
		< 10	31.8	5.6	0.10	1.34	1.46	0.19	0.22	15.4	5.3	3.03	90	70
		∅	33.3	5.9	0.10	1.21	1.38	0.18	0.31	13.2	4.3	3.10	101	78
10	Average (51-59)		33.8	6.2	0.11	1.27	1.40	0.18	0.26	13.3	4.5	3.37	110	87

Table A3 (cont.)

Analytical data of manganese nodules from area *F*.

Location	Station No.	Size mm	Mn	Fe	Co	Ni	Cu	Zn	Ba	SiO₂	Al₂O₃	U ppm	Ce ppm	La ppm
11	61 GB	10 - 20	33.8	4.7	0.09	1.17	1.45	0.22	0.26	13.2	4.4	3.43	100	80
		∅	33.8	4.7	0.09	1.17	1.45	0.22	0.26	13.2	4.4	3.43	100	80
	62 GB	20 - 40	35.3	6.6	0.10	1.11	1.20	0.16	0.24	16.8	6.3	3.34	115	90
		∅	35.3	6.6	0.10	1.11	1.20	0.16	0.24	16.8	6.3	3.34	115	90
	63 GB	60 - 80	29.0	5.4	0.12	1.08	1.02	0.17	0.27	14.7	5.7	2.06	110	100
		40 - 60	30.9	6.3	0.14	1.14	1.18	0.16	0.31	15.2	5.3	2.40	128	95
		∅	30.0	5.9	0.13	1.11	1.10	0.17	0.29	15.0	5.5	2.24	119	98
	63 GB+	60 - 80 outer zone	30.2	5.0	0.13	1.07	1.06	0.20	0.22	12.2	5.3	2.08	100	90
		core	28.1	5.5	0.13	0.95	0.96	0.18	0.26	15.8	5.8	1.67	105	80
	64 GB	10 - 20	33.1	5.0	0.09	1.23	1.42	0.20	0.25	13.9	4.8	3.38	95	80
		∅	33.1	5.0	0.09	1.23	1.42	0.20	0.25	13.9	4.8	3.38	95	80
	67 GB	10 - 20	32.1	5.0	0.08	1.21	1.45	0.20	0.25	15.8	5.3	–	135	80
		∅	32.1	5.0	0.08	1.21	1.45	0.20	0.25	15.8	5.3	–	135	80
11	Average (61-67)		32.9	5.4	0.10	1.17	1.32	0.19	0.26	14.9	5.3	3.10	113	86
12	70 GB	60 - 80	30.4	7.8	0.12	1.22	1.17	0.14	0.27	14.3	5.4	3.52	135	110
		20 - 40	32.1	7.6	0.13	1.23	1.21	0.16	0.29	13.2	4.7	3.51	135	110
		15 - 20	29.0	6.7	0.12	1.26	1.23	0.15	0.20	13.0	4.4	4.25	130	115
		10 - 15	31.0	7.5	0.13	1.34	1.31	0.15	0.19	16.5	5.3	3.15	115	80

Table A3 (cont.)
Analytical data of manganese nodules from area *F.*

Location	Station No.	Size mm	Mn	Fe	Co	Ni	Cu	Zn	Ba	SiO₂	Al₂O₃	U ppm	Ce ppm	La ppm
		5 - 10	28.4	8.5	0.14	1.27	1.22	0.13	0.20	18.7	5.7	2.78	140	80
		< 5	23.5	9.6	0.11	1.12	1.09	0.11	0.18	25.9	6.8	–	110	90
		∅	29.1	8.0	0.13	1.24	1.21	0.14	0.22	16.9	5.4	3.44	128	98
	71 GB	20 - 40	31.2	7.5	0.11	1.30	1.32	0.17	0.24	13.9	4.3	3.27	160	120
		15 - 20	32.0	7.0	0.12	1.34	1.36	0.17	0.20	14.0	4.9	3.27	110	80
		10 - 15	32.1	7.1	0.12	1.33	1.35	0.17	0.21	13.2	4.7	3.28	110	95
		5 - 10	30.6	7.6	0.13	1.31	1.30	0.16	0.19	15.7	5.9	3.00	110	100
		< 5	27.3	8.5	0.13	1.25	1.21	0.14	0.20	19.9	5.8	–	100	80
		∅	30.6	7.5	0.12	1.31	1.31	0.16	0.21	15.3	5.1	3.21	118	95
	72 GB	15 - 20	34.4	5.0	0.10	1.27	1.43	0.23	0.21	10.7	4.2	3.77	85	90
		10 -15	34.3	5.4	0.11	1.31	1.46	0.21	0.21	12.2	4.4	3.55	115	80
		∅	34.4	5.2	0.11	1.29	1.45	0.22	0.21	11.5	4.3	3.66	100	75
	74 KAL	brok.nod.	30.7	8.2	0.13	1.24	1.15	0.16	0.18	16.1	5.7	2.90	140	100
		∅	30.7	8.2	0.13	1.24	1.15	0.16	0.18	16.1	5.7	2.90	140	100
	75 DK	60 - 80	31.8	6.6	0.10	1.04	1.19	0.18	0.46	13.9	3.6	2.51	100	110
		40 - 60	35.9	5.8	0.11	1.21	1.32	0.24	0.30	10.3	3.4	3.45	125	70
		20 - 40	34.2	4.9	0.10	1.23	1.44	0.22	0.24	11.6	4.5	3.47	118	90
		∅	30.7	8.2	0.13	1.24	1.15	0.16	0.18	16.1	5.7	2.90	140	100
	75 DK	60 - 80	31.8	6.6	0.10	1.04	1.19	0.18	0.46	13.9	3.6	2.51	100	110
		40 - 60	35.9	5.8	0.11	1.21	1.32	0.24	0.30	10.3	3.4	3.45	125	70
		20 - 40	34.2	4.9	0.10	1.23	1.44	0.22	0.24	11.6	4.5	3.47	118	90
		∅	34.0	5.8	0.10	1.16	1.32	0.21	0.33	11.9	3.8	3.14	114	90

Table A3 (cont.)
Analytical data of manganese nodules from area *F.*

Location	Station No.	Size mm	Mn	Fe	Co	Ni	Cu	Zn	Ba	SiO₂	Al₂O₃	U ppm	Ce ppm	La ppm
12	Average (70-75)	∅	31.8	6.9	0.12	1.25	1.29	0.17	0.23	14.3	4.9	3.27	120	92
13	76 GB	15 - 20	34.7	6.4	0.12	1.40	1.44	0.22	0.22	10.3	4.0	3.44	117	85
		10 - 15	31.0	7.2	0.12	1.42	1.37	0.16	0.20	17.2	6.0	2.88	105	90
		5 - 10	25.2	7.9	0.12	1.20	1.16	0.13	0.20	24.4	7.8	–	115	90
		∅	31.4	7.0	0.12	1.36	1.35	0.17	0.21	17.3	5.9	3.16	112	88
	77 GB	40 - 60	35.7	6.2	0.12	1.22	1.31	0.19	0.36	10.0	3.3	2.92	140	90
		20 - 40	34.4	6.2	–	1.35	1.42	–	–	–	–	–	–	–
		15 - 20	30.5	7.5	0.13	1.31	1.34	0.15	0.20	16.8	5.9	2.95	120	120
		10 - 15	32.7	6.6	0.12	1.38	1.41	0.16	0.21	12.9	5.7	–	110	100
		5 - 10	31.3	7.2	0.12	1.41	1.39	0.15	0.21	14.5	5.0	3.08	113	100
		∅	32.9	6.7	0.13	1.33	1.37	0.16	0.25	13.6	5.0	2.98	121	103
	78 GB	80 - 100	34.3	5.5	0.10	1.08	1.04	0.22	0.38	12.5	3.1	2.04	100	100
		20 - 40	35.1	6.3	0.10	1.22	1.34	0.18	0.29	11.4	3.8	3.27	115	90
		15 - 20	31.1	6.3	0.09	1.25	1.41	0.18	0.20	17.6	5.7	2.97	105	90
		10 - 15	35.8	5.1	0.10	1.33	1.53	0.21	0.21	10.7	4.3	–	115	80
		∅	34.1	5.8	0.10	1.22	1.33	0.20	0.27	13.1	4.2	2.76	109	90
13	Average (76-78)		32.8	6.5	0.12	1.30	1.35	0.18	0.24	14.7	5.0	2.97	114	94
14	81 GB	60 - 80	30.9	7.5	0.11	1.10	1.23	0.15	0.42	15.0	3.8	2.54	100	90
		5 - 15	34.2	5.1	0.09	1.29	1.48	0.21	0.22	12.5	4.6	3.44	95	90
		∅	32.6	6.3	0.10	1.20	1.36	0.18	0.32	13.8	4.2	2.99	98	90

Table A3 (cont.)
Analytical data of manganese nodules from area *F*.

Location	Station No.	Size mm	Mn	Fe	Co	Ni	Cu	Zn	Ba	SiO₂	Al₂O₃	U ppm	Ce ppm	La ppm
	83 GB	10 - 30	32.4	6.2	0.11	1.28	1.38	0.19	0.20	13.6	5.0	3.25	100	100
		ø	32.4	6.2	0.11	1.28	1.38	0.19	0.20	13.6	5.0	3.25	100	100
	84 GB	20 - 40	25.7	9.1	0.10	1.09	1.13	0.12	0.22	24.8	6.8	2.73	140	90
		15 - 20	31.7	7.2	0.13	1.25	1.29	0.17	0.22	14.3	5.0	3.46	120	90
		10 - 15	30.8	7.8	0.13	1.33	1.33	0.16	0.19	16.1	5.1	3.00	105	100
		5 - 10	23.1	10.5	0.12	1.15	1.13	0.12	0.17	27.0	6.8	2.12	105	80
		ø	27.8	8.7	0.12	1.21	1.22	0.14	0.20	20.6	5.9	2.83	118	90
	85 GB	20 - 40	30.7	7.0	0.12	1.26	1.32	0.18	0.20	14.7	5.4	3.22	115	70
		10 - 15	33.4	6.8	0.12	1.33	1.36	0.19	0.20	12.2	4.6	3.40	110	80
		5 - 10	29.2	8.0	0.14	1.37	1.33	0.15	0.19	17.2	5.6	2.97	100	80
		ø	31.1	7.3	0.13	1.32	1.34	0.18	0.20	14.7	5.2	3.20	108	77
	87 GB	10 - 50	28.1	6.7	0.10	1.21	1.28	0.16	0.20	15.8	5.3	3.88	100	120
		ø	28.1	6.7	0.10	1.21	1.28	0.16	0.20	15.8	5.3	3.88	100	120
	88 GB	15 - 20	33.5	6.4	0.10	1.25	113)	0.21	80.18	12.2	4.6	83.55	95	90
		10 - 15	31.1	7.1	0.20	1.33	1.33	0.18	0.20	14.7	5.1	–	105	70
		5 - 10	26.0	8.3	0.20	1.26	1.24	0.13	0.20	23.3	7.1	–	100	80
		ø	30.2	7.3	0.17	1.28	1.31	0.17	0.19	16.7	5.6	3.55	100	80
	89 GB	80 - 100	28.2	8.4	0.14	1.12	1.14	0.14	0.27	16.5	4.7	2.56	125	110
		15 - 20	30.9	8.2	0.13	1.26	1.27	0.17	0.20	15.8	4.8	3.29	95	110
		5 - 15	28.6	9.2	0.14	1.29	1.24	0.14	0.19	19.7	5.5	2.85	105	100
		< 5	19.8	11.8	0.11	1.02	0.99	0.10	0.16	32.0	7.1	1.68	80	90
		ø	26.9	9.4	0.13	1.17	1.16	0.14	0.21	21.0	5.5	2.59	101	103

Table A3 (cont.)
Analytical data of manganese nodules from area *F*.

Location	Station No.	Size mm	Mn	Fe	Co	Ni	Cu	Zn	Ba	SiO₂	Al₂O₃	U ppm	Ce ppm	La ppm
14	Average (81-89)		29.9	7.5	0.12	1.24	1.29	0.17	0.22	16.6	5.2	3.18	104	94
15	93 GB	20 - 40	29.7	8.6	0.14	1.23	1.20	0.15	0.19	17.2	5.4	2.90	115	100
		15 - 20	33.5	7.3	0.14	1.29	1.31	0.15	0.20	17.6	5.3	3.23	100	100
		5 - 10	27.2	9.5	0.13	1.12	1.07	0.12	0.18	23.5	6.4	2.43	125	95
		ø	30.1	8.5	0.14	1.21	1.19	0.14	0.19	19.4	5.7	2.88	113	98
	94 GB	40 - 60	27.7	9.0	0.13	81.14	1.06	0.14	0.21	17.6	6.0	3.14	155	80
		20 - 40	30.0	8.7	0.13	1.20	1.20	0.18	0.18	12.3	4.7	3.23	100	90
		15 - 20	30.4	8.6e	0.13	1.23	1.23	0.16	0.18	15.1	5.2	3.01	125	100
		10 - 15	28.0	9.0	0.13	1.14	1.15	0.18	0.18	18.3	5.6	2.87	130	100
		5 - 10	25.9	9.8	0.14	1.13	1.12	0.13	0.18	21.4	6.3	2.51	125	80
		ø	28.4	9.0	0.13	1.17	1.15	0.15	0.19	16.9	5.6	2.95	127	90
	94 GB*	crust	11.4	13.4	0.08	0.62	0.62	0.07	0.13	39.7	8.6	1.10	90	110
	95 GB	20 - 40	29.2	8.1	0.12	1.18	1.13	0.15	0.18	19.0	6.1	3.06	105	100
		15 - 20	30.3	7.8	0.12	1.18	1.24	0.16	0.19	17.6	5.6	3.04	105	90
		10 - 15	28.9	9.0	0.13	1.22	1.22	0.15	0.19	20.0	5.9	2.90	105	90
		< 10	24.5	9.4	0.12	1.10	1.08	0.12	0.18	26.7	7.0	2.22	110	100
		ø	28.2	8.6	0.12	1.17	1.17	0.15	0.19	20.8	6.2	2.81	106	95
15	Average (93-95)		28.9	8.7	0.13	1.18	1.17	0.15	0.19	19.0	5.8	2.88	115	94
16	99 GB	40 - 60	33.3	11.3	0.12	1.16	0.99	0.18	0.27	10.6	5.8	3.73	130	100

Table A3 (cont.)
Analytical data of manganese nodules from area *F*.

Location	Station No.	Size mm	Mn	Fe	Co	Ni	Cu	Zn	Ba	SiO$_2$	Al$_2$O$_3$	U ppm	Ce ppm	La ppm
		20 - 30	34.3	11.4	0.12	1.19	1.05	0.17	0.27	10.6	5.6	3.68	110	100
		15 - 20	31.7	11.5	0.12	1.20	1.02	0.17	0.22	12.0	6.3	3.67	120	100
		10 - 15	32.1	11.5	0.12	1.31	1.12	0.17	0.20	10.6	6.0	3.68	120	100
		5 - 10	31.8	11.4	0.14	0.53	1.09	0.15	0.19	12.3	6.7	3.47	100	95
		< 5	29.5	12.5	0.15	1.21	1.07	0.14	0.20	14.8	8.2	–	115	80
		brok.nod.	33.8	10.7	0.11	1.15	1.03	0.18	0.25	9.9	5.5	3.79	115	90
		ø	32.4	11.5	0.13	1.11	1.05	0.17	0.23	11.5	6.3	3.67	115	95
	100 GB	brok.nod. (20 - 40)	35.7	10.7	0.09	1.09	1.01	0.20	0.25	9.9	5.0	3.67	110	90
		brok.nod. < 20	35.5	10.5	0.10	1.04	0.98	0.20	0.26	9.5	5.0	3.58	110	100
		ø	35.6	10.6	0.10	1.07	1.00	0.20	0.26	9.7	5.0	3.63	110	95
	101 GB	20 - 40	24.3	19.2	0.14	0.82	0.60	0.13	0.23	12.3	5.5	4.67	210	190
		brok.nod.	34.1	9.1	0.07	1.00	1.04	0.19	0.27	10.6	5.4	3.48	95	100
		ø	29.2	14.2	0.11	0.91	0.82	0.16	0.25	11.5	5.5	4.08	153	145
	102 GB	40 - 60	34.3	6.9	0.07	0.84	0.96	0.24	0.26	10.2	5.3	3.83	100	80
		ø	34.3	6.9	0.07	0.84	0.96	0.24	0.26	10.2	5.3	3.83	100	80
	107 GB	20 - 40	35.2	8.3	0.07	0.96	1.02	0.22	0.28	9.9	5.3	3.46	80	50
		ø	35.2	8.3	0.07	0.96	1.02	0.22	0.28	9.9	5.3	3.46	80	50
	108 GB	40 - 60	34.5	10.4	0.10	0.94	0.90	0.20	0.30	9.2	4.6	3.37	90	90
		20 - 40	34.5	11.6	0.11	1.08	0.93	0.19	0.29	9.2	4.8	3.43	128	110

Table A3 (cont.)
Analytical data of manganese nodules from area *F*.

Location	Station No.	Size mm	Mn	Fe	Co	Ni	Cu	Zn	Ba	SiO$_2$	Al$_2$O$_3$	U ppm	Ce ppm	La ppm
		< 20	33.0	12.1	0.13	1.18	0.96	0.16	0.27	11.3	5.3	3.45	120	90
		brok.nod. 20 - 40	35.0	11.0	0.11	1.03	0.90	0.20	0.28	8.8	4.6	3.44	120	90
		brok.nod. < 20	34.1	11.5	0.12	1.11	0.96	0.17	0.29	9.9	5.2	3.53	130	120
		ø	34.3	11.4	0.11	1.07	0.93	0.18	0.29	9.7	4.9	3.44	118	100
	109 GB	40 - 60	33.7	11.5	0.11	1.05	0.84	0.18	0.32	10.6	4.6	3.20	110	100
		20 - 40	33.2	12.0	0.12	1.07	0.88	0.17	0.31	10.6	5.0	3.30	115	100
		10 - 15	32.3	12.8	0.13	1.14	0.94	0.15	0.28	11.7	5.3	3.37	135	100
		brok.nod.	33.3	11.4	0.10	1.01	0.82	0.20	0.30	9.9	4.1	3.25	135	120
		ø	33.1	11.9	0.12	1.07	0.87	0.18	0.30	10.7	4.8	3.28	124	105
	110 KG	40 - 60	34.9	11.0	0.11	0.94	0.85	0.19	0.30	10.2	4.4	3.18	100	100
		20 - 40	33.5	11.8	0.11	1.03	0.85	0.18	0.31	9.5	4.7	3.30	125	100
		brok.nod.	34.4	11.2	0.10	1.06	0.84	0.19	0.31	9.5	4.4	3.15	110	100
		ø	34.3	11.3	0.11	1.01	0.85	0.19	0.31	9.7	4.5	3.21	112	100
16	Average (99-110)		33.6	10.8	0.10	1.00	0.94	0.19	0.27	10.4	5.2	3.58	115	99

*These samples not included in average values.